

# Realisation and evaluation of a start-stop journal bearing test-rig

MARCUS GRALDE  
TÓMAS RÚNAR SÖLVASON

Master of Science Thesis  
Stockholm, Sweden 2014



**KTH Industrial Engineering  
and Management**



# Realisation and evaluation of a start-stop journal bearing test-rig

Marcus Gralde  
Tómas Rúnar Sölvason



Master of Science Thesis MMK 2014:22 MKN 112  
KTH Industrial Engineering and Management  
Machine Design  
SE-100 44 STOCKHOLM





KTH Industriell teknik  
och management

## Examensarbete MMK 2014:22 MKN 112

### Realisering och utvärdering av en glidlagerrigg för start-stop-provning

Marcus Galde

Tómas Rúnar Sölvason

Godkänt 2014-juni-11	Examinator Ulf Sellgren	Handledare Stefan Björklund
	Uppdragsgivare Scania CV AB	Kontaktperson Christer Spiegelberg

## Sammanfattning

Även om en betydande mängd forskning inom glidlager och fullfilmslager har genomförts så är med dagens datorkapacitet en stor del av resultaten numera teoretiska eller simulerade. Medan Scania producerar experimentella resultat, så är dessa dyra och tidskrävande. Vidare är det ibland svårt att hålla en tillräckligt kontrollerad miljö för att dra slutsatser från proverna. Med en dedikerad testrigg som kan tillförlitliga resultat tas fram billigare och snabbare.

Detta examensarbete är en fortsättning av kursen *Avancerad Maskinkonstruktion* som ges vid Kungliga Tekniska Högskolan. Under detta examensarbete har testriggen tillverkats, byggts och utvärderats. Vidare har programvara för testriggen utvecklats.

Informationssökning gjordes på glidlager, fullfilmslager, riskbedömning och signalbrushhantering. Mekanisk utveckling har gjorts i Autodesk Inventor, medan Matlab användes för mjukvaruutveckling. Faktorial design har nyttjats vid utformningen av tester. Resultaten jämfördes med en enkel teoretisk modell.

Testresultaten visade lovande resultat för Stribeck kurva-producerande tester, med god likhet till kända friktionsvärden och trender. Testriggen visade god reproducerbarhet vid replikerade tester. Testriggen producerar slitage på samtliga testade lagerytor.

Under ett längre test så har axel och stödlager skadats, varför service behövs för att testriggen skall vara i brukbart skick.

Testriggen kräver ytterligare verifiering, men resultaten från de prov som genomförts visar att test-riggen ger värdefull och tillförlitlig information om slitage och friktion kunna utrönas.

Nyckelord: glidlager, hydrodynamisk smörjfilm, nötning, start-stop, testrigg





KTH Industrial Engineering  
and Management

Master of Science Thesis MMK 2014:22 MKN 112

## Realisation and evaluation of a start-stop journal bearing test-rig

Marcus Galde  
Tómas Rúnar Sölvason

Approved 2014-june-11	Examiner Ulf Sellgren	Supervisor Stefan Björklund
	Commissioner Scania CV AB	Contact person Christer Spiegelberg

### **Abstract**

While there has been substantial body of work in the field of journal bearing research, much of it is today theoretical or simulated due to today's computing power. Scania produces experimental data from motor testing, but these are expensive and time consuming. Furthermore there is a difficulty in keeping a sufficiently controlled environment, which at times makes it hard to draw conclusions from testing results. They therefore wish to develop a test-rig which can evaluate friction and wear in journal bearings.

This thesis is a continuation of a project in the course *Advanced Machine Design* given at KTH Royal Institute of Technology. During this thesis the test-rig has been manufactured, built, and evaluated. Furthermore software for the test-rig was developed.

Information on journal bearings, risk assessment and signal noise handling were sought. Mechanical development was done with Autodesk Inventor, while Matlab was used for software development. Factorial design was utilised when designing tests and compared to a simple theoretical model.

Test results showed promising results for Stribeck curve-producing tests, with good resemblance to known frictional values and trends. Furthermore the test-rig showed good repeatability for replicated tests and produced wear on the bearing shells used. During a prolonged test, the shaft and support-bearings were damaged and requires servicing to be in an operational state.

The test-rig requires to be further verified, but the tests that were carried out showed valuable and reliable information on wear and frictional values.

Keywords: journal bearing, hydrodynamic lubrication, wear, start-stop, test-rig



## FOREWORD

---

*In this chapter we give credit to everybody who has contributed to this thesis.*

Firstly we would like to thank our supervisor at Scania, Christer Spiegelberg, for his guidance and invaluable support, but as well for his never-ending enthusiasm and high spirit. We would also like to thank our supervisor at KTH, Stefan Björklund, for his guidance and trust afforded to us. To both of you we would like to extend a thank you.

We would like to thank Mikael Källberg for all his help with the electrical side of the thesis. Especially during the later stages of the project, your help was invaluable. Your friendship is greatly appreciated.

At KTH we would like to thank Tomas Österberg and Jan Stamer for their assistance with manufacturing.

At Scania we additionally want to thank Hubert Herbst and Christoffer Rinderström for their suggestions and input during the initial phases of this thesis.

Lastly we would like to thank our families for the support during our studies at KTH. Rebekka Karlsdóttir, Tómas girlfriend gets special thanks for the excellent lunchboxes and her tolerance for the late nights.

Marcus Gralde & Tómas Rúnar Sölvason

Stockholm, June 2014



# NOMENCLATURE

Here notation, abbreviations and programs used in this thesis are listed.

## Notations

<b><i>Symbol</i></b>	<b><i>Description</i></b>	<b><i>Unit</i></b>
$C$	Radial clearance	[m]
$D$	Diameter	[m]
$e$	Eccentricity	[-]
$F$	Force	[N]
$F_0$	Dimensionless load	[-]
$h$	Average film thickness	[m]
$h_0$	Minimum film thickness	[m]
$L$	Bearing length	[m]
$n$	Velocity	[rpm]
$p$	Pressure	[Pa]
$R$	Radius	[m]
$Re$	Reynolds number	[-]
$R_q$	Surface roughness	[m]
$U$	Relative speed	[m/s]
$u$	Peripheral speed	[m/s]
$V$	Wear volume	[m <sup>3</sup> ]
$V_c$	Overlapping volume	[m <sup>3</sup> ]
$\eta$	Dynamic viscosity	[Pa·s]
$\lambda$	Film parameter	[-]
$\mu$	Friction coefficient	[-]

$\rho$	Density	[kg/m <sup>3</sup> ]
$\tau$	Shear stress	[MPa]
$\omega$	Angular velocity	[rad/s]

## Abbreviations

### ***Abbreviation*   *Keyword***

---

<i>AMD</i>	Advanced Machine Design
<i>CAD</i>	Computer Aided Design
<i>CMM</i>	Coordinate Measurement Machine
<i>DAQ</i>	Data Acquisition System
<i>EMC</i>	Electro Magnetic Compatibility
<i>EMI</i>	Electro Magnetic Interference
<i>EMR</i>	Electro Magnetic Radiation
<i>FMEA</i>	Failure Mode Effects Analysis
<i>GUI</i>	Graphical User Interface
<i>KTH</i>	The Royal Institute of Technology
<i>NI</i>	National Instruments
<i>OPC</i>	OLE for Process Control
<i>PLC</i>	Programmable logic control
<i>RMS</i>	Root mean square

### ***Programs and Software***

---

*IndraWorks Engineering*

*Autodesk Inventor*

*Matlab*

# TABLE OF CONTENTS

---

<b>1. INTRODUCTION.....</b>	<b>1</b>
1.1. Background.....	1
1.2. Purpose .....	1
1.3. Limitations.....	1
1.4. Methods .....	2
<b>2. FRAME OF REFERENCE.....</b>	<b>3</b>
2.1. Bearings .....	3
2.2. Principle of friction measurement .....	10
2.3. Measure wear.....	10
2.4. Safety .....	13
2.5. Electrical noise .....	14
<b>3. PREVIOUS WORK.....</b>	<b>17</b>
3.1. General test-rig description .....	21
3.2. The test cell.....	26
3.3. Status at end of Advanced Machine Design course .....	26
<b>4. CHANGES AND IMPLEMENTATION .....</b>	<b>27</b>
4.1. Electrical cabinet .....	27
4.2. Risk Assessment.....	27
4.3. Safety-measures.....	28
4.3.1. Door breakers .....	28
4.3.2. Safety cover.....	28
4.3.3. Splash cover breaker .....	29
4.3.4. Pump breaker.....	29
4.3.5. Insulation.....	29
4.3.6. Loaded spring .....	30
4.3.7. Emergency stop buttons .....	30
4.4. Assembly .....	31
4.4.1. Process.....	31
4.4.2. Assembly of power train .....	31
4.4.3. Assembly of loading mechanism .....	33

4.4.4.	Assuring mechanical repeatability .....	33
4.4.5.	Assembly of oil system .....	35
4.4.6.	Installation of electrical cabinet .....	35
4.5.	Software.....	36
4.5.1.	Method .....	36
4.5.2.	Servo controller .....	36
4.5.3.	Features .....	37
<b>5.</b>	<b>INITIAL TESTING AND EVALUATION .....</b>	<b>39</b>
5.1.	Electrical wiring .....	39
5.2.	Noise and spikes in gathered data.....	39
5.3.	Friction torque load cell misalignment.....	42
5.4.	Oil splash .....	43
5.5.	Assembly and disassembly of test-bearing housing .....	45
5.6.	Oil splash safety breaker.....	47
5.7.	Performance of oil system .....	49
5.8.	Evaluation of friction measurement concept .....	49
<b>6.</b>	<b>TESTING.....</b>	<b>51</b>
6.1.	Stribeck curve test .....	51
6.2.	Wear test .....	52
6.3.	Wear progress test .....	53
<b>7.</b>	<b>RESULTS .....</b>	<b>55</b>
7.1.	Stribeck curve test .....	55
7.2.	Wear test and subsequent damage of test-rig .....	60
<b>8.</b>	<b>DISCUSSION AND CONCLUSION .....</b>	<b>63</b>
8.1.	Discussion.....	63
8.2.	Conclusions .....	64
<b>9.</b>	<b>FUTURE WORK .....</b>	<b>65</b>
<b>10.</b>	<b>REFERENCES .....</b>	<b>67</b>
<b>Appendix A.</b>	<b>SIZE DRAWINGS.....</b>	<b>A.1</b>
<b>Appendix B.</b>	<b>TESTING PLAN FOR STRIBECK CURVE TEST.....</b>	<b>B.1</b>

# 1. INTRODUCTION

---

*This chapter describes the background, purpose, goal, limitations and methods used for this work.*

## **1.1. Background**

This work has been produced as a master thesis at the *Department of Machine Design at KTH, The Royal Institute of Technology*. This thesis is a continuation of a project that was initiated during the *Advanced Machine Design course (AMD-course)* as part of the Machine Design master program at the *Department of Machine Design*. The project is a joint collaboration between the Swedish truck manufacturer Scania CV AB and KTH where the deliverable is a journal bearing test rig.

During the AMD course a group of four students along with Scania formulated the scope the project, defined the requirements and generated and evaluated concepts. The chosen concept was worked into a detailed design and by the end of the course a complete CAD model of the test rig was delivered, along with detailed drawings and all necessary documentation needed for manufacturing. The original deliverable from the course was a fully functioning test rig, but as the project progressed the scope of the project was too large for the given timeframe. Two months before the deadline of the course it was decided that this project should be continued as a master thesis. This allowed the group to focus on delivering well thought through solutions and a solid foundation for future work to be built upon.

There has been a substantial amount of work in the field of bearing research; much of it is theoretical or simulated (Simmons, 2010, p. 1). It is of Scania's interest to, in a less expensive and time consuming manner, gain further knowledge on bearing performance in internal combustion engines.

## **1.2. Purpose**

Scania wants the ability to evaluate friction and wear in hydrodynamic bearings under stopping and starting conditions without burdensome and costly full-motor testing. The goal is to allow quick and cost-effective deployment of automated tests in a test rig that gives the ability to control different input parameters. The purpose of this thesis work is to deliver a test-rig which fulfils Scania's requirements for delivering additional experimental results to their body of theoretical and simulated results.

## **1.3. Limitations**

A major limitation for this project is time, but also budgeting constraints. Because of the time constraint some of the limitations were determined *during* the project. These limitations were:

- The test rig is not developed for placement at Scania
- Multiple tests will not be performed
- Creating a theoretical model in AVL Excite
- The evaluated bearing has the same size as the bearing found in a balance shaft module in a DL5 Scania engine.

To develop the test rig for placement at Scania would require following Scania's standard on wire markings, resulting in more expensive manufacturing cost and even longer delivery time of the electrical cabinet that accompanies the test rig. The AVL Excite model was intended to be used for evaluation of the real test data from the test rig, after multiple tests had been run. Since time constraints did not allow multiple tests to be performed, the a simpler model comparison was done instead.

## **1.4. Methods**

The thesis started with a pre-study in which information on journal bearings, risk assessment, data acquisition (DAQ) and signal noise handling was sought. Problems were then broken down to sub-tasks, where requirements were drawn up and pre-study knowledge, together with discussions with Scania, sub-contractors and experts were used to generate possible solutions to the sub-problems. These were then evaluated and implemented.

Risk assessment for the thesis itself was done in accordance to failure mode effect analysis (FMEA), as described by Harvey Maylor in the book Project Management (Maylor, 2010). Risk assessment for the test-rig was done with the method described in EN ISO 13849-1, as described by Jokab ABB's condensed publication (ABB AB Jokab Safety, 2011).

The risk assessment for the project was partly used for planning, so occurrence of possible risks could be reduced or avoided. A time plan was constructed in cooperation with Scania and set up as a Gantt chart and continuously reviewed.

Both during the AMD-course and the thesis project all design concepts and detailed designs were developed with the CAD-software Autodesk Inventor. The software to control the test rig and acquire data was loosely developed according to the SCRUM method and programmed in Matlab with a bottom-up approach.

A weekly progress report, detailing the progress of the project and everything related to it, was made in the form of short bullet points and sent to supervisor on a weekly basis. In addition to the weekly reports, meetings were scheduled when thorough discussions about some aspects of the project were needed.

Factorial design was used to design tests, with replications added when possible from a time plan point-of-view. Local regression was used to analyse the collected data. The result was then compared to a simple theoretical model.

## 2. FRAME OF REFERENCE

---

*In this chapter the frame of reference of the work is discussed.*

### **2.1. Bearings**

The simplest form of a bearing is a bored out hole which constrains a shafts (journal) movement, while facilitating its rotation. Bearings may be lubricated with grease or oil in order to lower the frictional value or in plastic bearings include a filler material. Popular fillers include Molybdenum sulphide ( $\text{MoS}_2$ ), Polytetrafluoroethylene (PTFE), Polyethylene (PE) and graphite. The main reason for including filler material is to increase material compatibility by building a dry lubrication film, thus reducing wear and frictional value (Beek, 2009, p. 250).

These simple bearings are popular when low forces and speeds are involved, such as in door-hinges, household appliances or toys. Plastic bearings are particularly popular in food processing where contaminants, such as oil, are not allowed. Common for both metal-metal and metal-plastic bearings is that they are dimensioned with the help of a pV-value (Pressure Velocity), which is graphed for the predetermined allowable wear per hour, ensuring that the bearing does not overheat.

While simple greased steel-on-steel bearings and plastic bearings are well documented and cheap, they do not allow for high speed or high loads. When considering higher speeds, higher loads or lower losses, one often instead considers rolling-element bearings, hydrodynamic bearings or even magnetic bearings.

Hydrodynamic bearings look similar to dry bearings but instead operate on the principle that oil is continuously dragged in between the surfaces to the degree that the journal and bearing separate from each other. Hydrodynamic lubrication is commonly exemplified with aquaplaning, where water is forced into the contact zone between tire and asphalt by the tire. This builds up pressure until contact between the tire and asphalt is lost, resulting in lost control of steering. While aquaplaning primarily relies on speed, the dominating variable for hydrodynamic lubrication is instead the applied force. There are three main requirements that need to be fulfilled in order to allow a hydrodynamic regime. Firstly surfaces need to be converging, in other words, the surfaces need to create a wedge. This is created by the clearance between shaft and bearing and the offset caused by the weight of the shaft, as seen in Figure 1. Secondly there needs to be a relative motion between the surfaces and lastly a viscous fluid present between the surfaces. The ratio  $C/R$ , as described in Figure 1, of hydrodynamic journal bearings is commonly in the order of  $10^{-3}$  (Harnoy, 2003, p. 162).

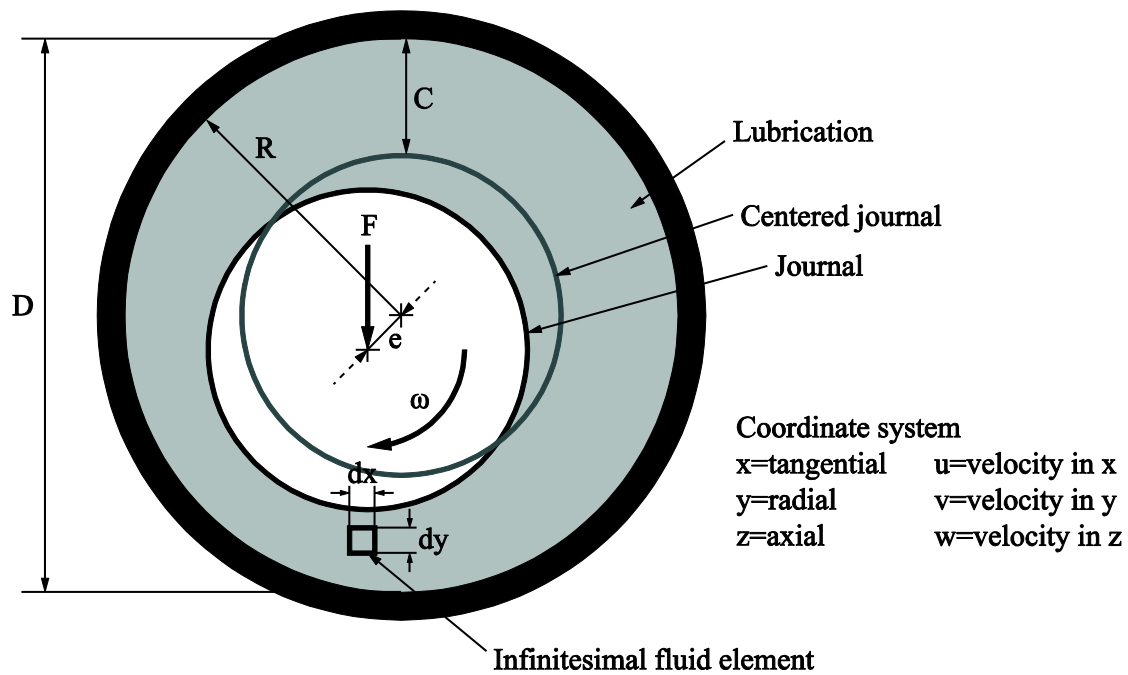


Figure 1. Schematic illustration of a journal bearing

Hydrodynamic lubrication allows for almost unmatched low friction in a journal bearing, as low as 0.01-0.001 (Beek, 2009, p. 274). The main source of friction in hydrodynamic lubrication is due to the shearing of the lubricant. The journal bearing is beaten in low friction only by bearings which are separated by lower density matters such as air or even vacuum, such as air bearings or magnetic bearings. As in aquaplaning, there is a need for a velocity and pressure in order to build the oil film thickness and allow for operation in the hydrodynamic lubrication regime.

The build-up to hydrodynamic regime is preceded by two lubrication regimes, the boundary lubrication and mixed lubrication regime. Boundary lubrication is similar to the simplest form of bearings, where the asperities of the mating surfaces bear the load. Operating at this regime causes the highest frictional value and highest wear rate for a given bearing. Mixed lubrication regime on the other hand divides the load carrying capacity between the asperities and the lubrication, which at this point has built up sufficient pressure to bear part of the load. The mixed lubrication regime allows for lowered frictional value until hydrodynamic lubrication has been achieved. It can be seen as a transition composed of both the boundary and hydrodynamic regimes where the proportion of dominating regime quickly shifts from one to the other, as described in Figure 2.

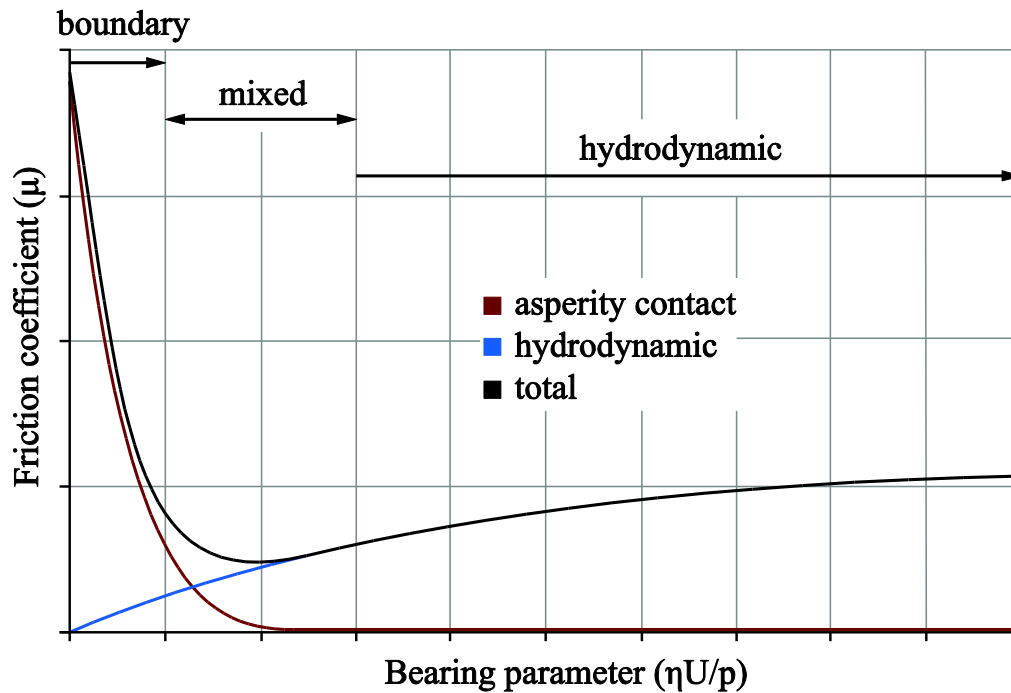


Figure 2. Stribeck curve showing the different components of the total friction (Tomanik & Ferrarese, 2006)

This also implies that one cannot reach hydrodynamic lubrication without passing the boundary and mixed lubrication regimes and that each occurrence causes wear to the bearing. For journals where this is unacceptable, such as in turbines, this is commonly solved by employing hydrostatic bearings, where the pressure is supplied to bearing with a pump, thus reducing wear.

The hydrodynamic regime ideally allows for no wear to take place and a reliable frictional value, but realistically wear particles from earlier regimes are not completely removed from the lubricant, which may cause wear. These particles are often hard, broken off, asperities or dust that has not been carried away by the lubricant. Since these particles have been sheared off and work hardened they are very hard.

In the early days of journal bearings, water lubricated hard wood bearings were used. In 1839 Isaac Babbitt patented (Babbitt, 1839) the tin-based metal alloy white metal, commonly referred as Babbitt metal. This alloy allowed for low friction, good embedability of particles, good resistance to galling (a form of adhesive wear) and low manufacturing cost. Good embedability is critical in order to reduce wear to the shaft, which is often costly to replace. For this reason the shaft is often hardened, which reduces wear and further increases compatibility. Furthermore the embedability infers that the bearing is softer than the journal, which allows for some conforming to machining and alignment errors. The low friction and galling resistance are coupled and are due to the good compatibility of the steel journal and Babbitt surface. It is instead estimated that for a correctly designed bearing abrasive wear, where hard asperities or particles plough the bearing material, accounts for 85% of the wear (Harnoy, 2003, p. 274). Babbitt however has a relatively low melting point and loses much of its compressive strength at elevated temperatures. The Babbitt is today bonded to a steel or aluminium shells as a liner, as seen in Figure 3, where automotive engines have a liner of a thickness below 800  $\mu\text{m}$  (Harnoy, 2003, p. 280).



Figure 3. Steel bearing shells with aluminium liner from a Scania DL5 balance shaft module

This allows for the heat to be more effectively transferred away and a general trend has been to reduce the thickness of the Babbitt liner as this allows for better resistance against creep and fatigue, as seen in Figure 4.

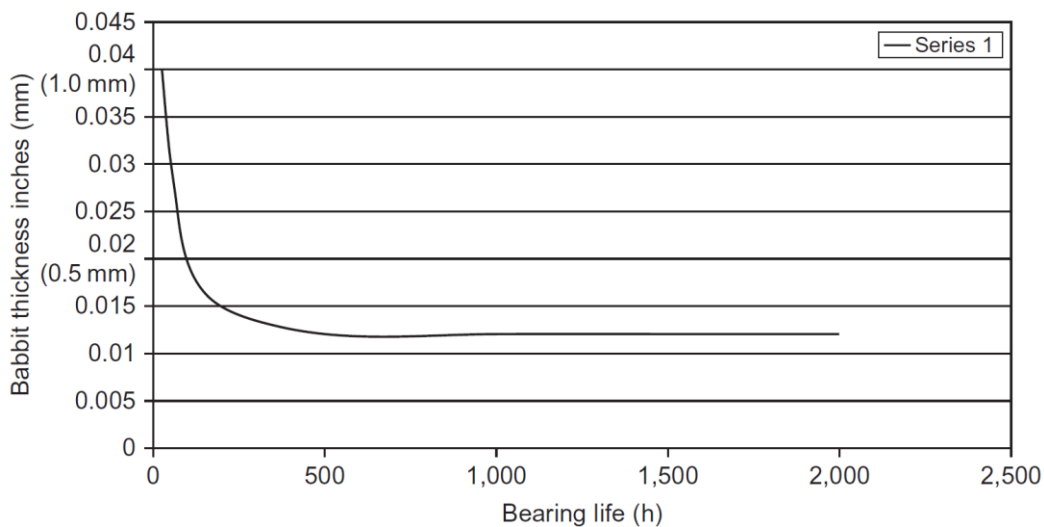


Figure 4. Life of bearing plotted against thickness of Babbitt liner (*Gas Turbine Engineering Handbook, Fourth Edition, 2011*)

Should oil starvation take place during operation it often results in catastrophic seizure of the bearing, due to the lubricant being the primary source of transporting heat away from the bearing. Heat builds up, softening the Babbitt, which in turn reduces its mechanical properties, leading to a run-away process towards failure. For this reason critical machinery require costly lubrication systems. Internal combustion engines operate at levels above 100 °C, at which point the white metals lose almost 50 % of their compressive strength (Harnoy, 2003, p. 279).

While the internal combustion engine can take between half a second to four seconds to start, the oil pressure can take up to eight seconds to build up, exacerbating wear of the journal bearings during start-up (Gudin, Mian, & Sanders, 2013). This is further aggravated by the fact that the chock-load of a cylinder firing may happen during this period.

When designing hydrodynamic journal bearings the important design parameters are obtained by solving Reynolds equation. This partial differential equation was derived by Osborne Reynolds in 1886 from the Navier-Stokes and continuity equations, which describe fluid in

motion. The Navier-Stokes equation applies Newton’s second law of motion onto an infinitesimal fluid element, as seen in Figure 5.

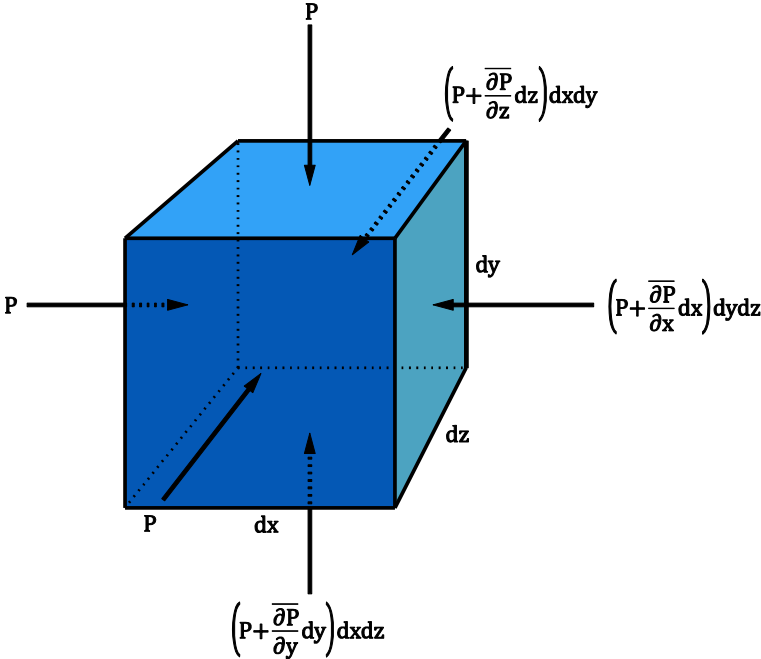


Figure 5. Infinitesimal fluid element

This is applied to a range of problems, such as modelling flow around airplane wings and flow in pipes. Since the Navier-Stokes equations are time consuming to solve, Reynolds derived a simplified equation with nine key assumptions. Firstly (1), it is assumed that the lubricant is Newtonian, continuous and incompressible. This means that the shear stress of the fluid is related to the strain in a linear manner, see equation (1); the more the fluid is distorted, the more it is being sheared.

$$\tau = \eta \frac{du}{dy} \tag{1}$$

Most fluids are Newtonian, including mineral oils and synthetic oils. There has however been some research (Mokhiamer, Crosby, & El-Gamal, 1998) which suggests that lubricants with polymer additives, which behave as a non-Newtonian fluid, increased the load-carrying capacity and also reduced the friction factor of a journal bearing. Taking this into account could then be beneficial for evaluating a bearing design where such a lubricant is used. Furthermore the assumption of a continuous fluid may not always be fulfilled, as there are always some air bubbles that are soluble in reality. This is negligible in practice, unless there is fluid cavitation (the vapour pressure is higher than the lubricants pressure) or foaming. Commonly anti-foaming additives are added to lubricants to reduce the problem, while cavitation is lessened by ensuring that the ambient pressure is sufficiently high.

Secondly (2) it is assumed that the fluid film flows in a laminar fashion. In fluid dynamics the Reynolds number is used to estimates the ratio between inertial and viscous forces, with a low

Reynolds number equating a laminar flow. For a fluid film-flow the Reynolds number is expressed as

$$Re = \frac{U\rho h}{\eta} \quad (2)$$

Where  $h$  is the average film thickness,  $\rho$  is the fluid density,  $U$  is the relative speed and  $\eta$  is the fluids dynamic viscosity. Reynolds numbers smaller than 1,000 are considered fully laminar. A small Reynolds number is also the case for most practical implementations of journal bearings (Harnoy, 2003, p. 69).

Thirdly (3) the fluid is assumed to adhere to the boundary surfaces and travel at the same velocity at these surfaces. This is commonly called a no-slip assumption.

The remaining assumption rest on order analysis of the equations terms, where terms with relative lower order of magnitude can be assumed to have negligible effect on the result in relation to the higher order terms. These assumptions can be condensed to:

4. The  $v$ -velocity component, as shown in Figure 1, in the bearing is negligible in comparison to  $u$  and  $w$ .
5. The velocity gradient in  $u$  and  $w$  are negligible in comparison to  $v$ .
6. The pressure across  $v$  is constant, due to the thickness of the fluid film
7. The effect of curvature of the journal bearing on pressure and flow is neglected, since the film thickness is so small in comparison to the radius.
8. The force of gravity on the fluid is so small in comparison to viscous forces that it is neglected.
9. The fluid inertia is small in comparison to the viscous forces and thus neglected. This is often justified by a low Reynolds number.

For most practical bearings the surfaces are assumed as rigid and the viscosity is assumed to be constant, with the viscosity determined by the oil properties coupled with the average temperature of the incoming and outgoing lubricant flow in the bearing. This significantly simplifies the Reynolds equation. Analytical answers for infinitely long and short bearings become possible with these assumptions, while other  $L/D$ -ratios are solved numerically. Historically long bearings, as defined by  $L \gg D$ , were favoured, but short bearings are widely used today. Short bearings are less sensitive to misalignment due to its shorter length, exhibit better heat transfer because increased side leakage and less wear as particles are removed at an increased rate. In 1958 Raimondi and Boyd produced dimensionless charts for finite-length bearings. These charts present various performance parameters for designing a bearing, such as the Sommerfeld number, making it comparatively easy to design journal bearings.

Today advanced computer software is heavily employed to design and simulate journal bearing, which can take into account previously simplified assumptions, such as the bearings surface compression, as well as surface topology.

None the less, the likelihood of attaining a full film lubrication regime can easily be assessed by a few calculations.

The dimensionless film parameter,  $\Lambda$ , is defined as:

$$\Lambda = \frac{h_0}{\sqrt{(Rq_1^2 + Rq_2^2)}} \quad (3)$$

Where  $h_0$  is the minimum film thickness and  $Rq$  is the RMS-average roughness of the shaft and bearing shells. It can be understood that the film thickness needs to be larger than the average roughness, and a fully developed hydrodynamic film is said to be fully built at a  $\Lambda$  of approximately 3-4 (Beek, 2009, p. 276). The minimum film thickness is calculated with the equation (4) (Eriksson, Folkesson, & Hagman, 2001).

$$h_0 = (1 - e) \cdot C \quad (4)$$

The relative eccentricity,  $e$ , is calculated with equation (5).

$$e = \frac{1}{5} \cdot \log \left( \frac{1 + \left(\frac{2R}{L}\right)^2 \cdot F_0}{0.3} \right) \quad (5)$$

Where  $F_0$  is the dimensionless load, calculated by equation (6).

$$F_0 = \frac{F}{W \cdot u \cdot \eta} \cdot \left(\frac{C}{R}\right)^2 \quad (6)$$

Where the peripheral speed,  $u$ , is calculated with equation (7).

$$u = \omega \cdot R \quad (7)$$

The dimensionless film parameter,  $\Lambda$ , gives a rough approximation to the likelihood of hydrodynamic lubrication being present.

## 2.2. Principle of friction measurement

During the AMD-course a few concepts on how to implement the friction measurement mechanism were evaluated. The chosen concept was heavily influenced by the Eindhoven bearing test-rig which uses a method of loading the bearing that is able to shear. This allows measuring of the frictional torque between the shaft and the bearing, as seen in Figure 6.

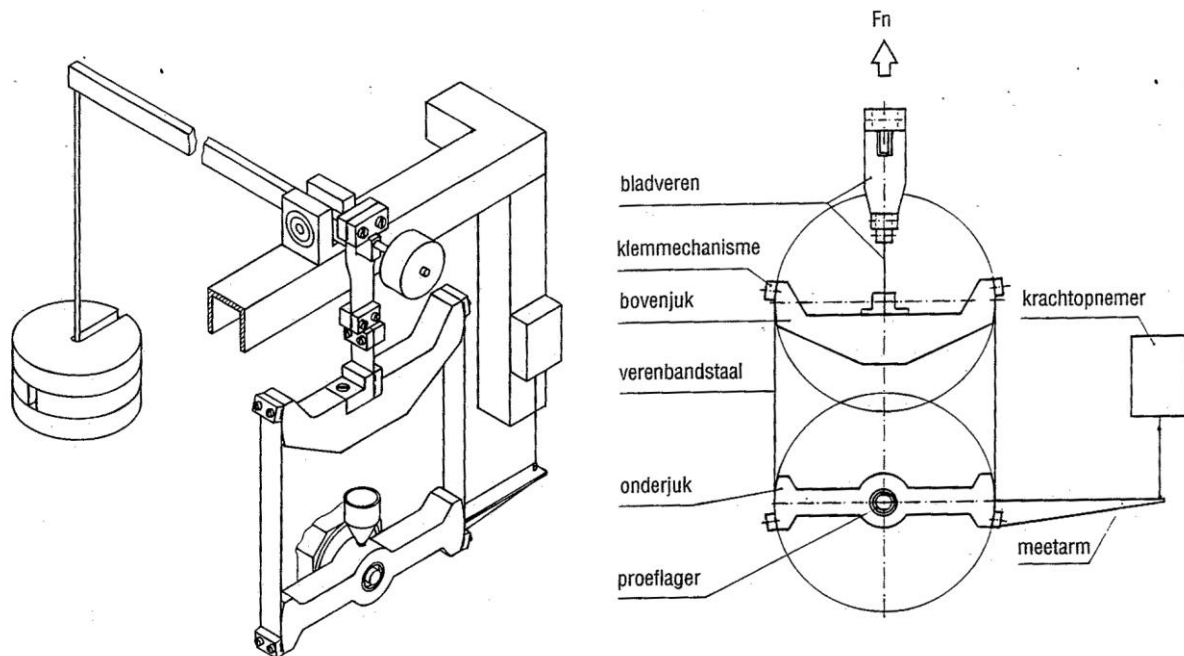


Figure 6. The principle of which the Eindhoven bearing test rig operates (Peels & Meesters, 1996)

The system employs two yokes that are connected by two thin sheet metal pieces. The two yokes both have radiuses that allow for them to turn, winding up or down the sheet metal around its radius. This allows the yokes to shear when a torque is applied at the bearing (proeflager), which is measurable with an arm coupled to a force-sensor, as seen on the right of Figure 6. Furthermore, the loading-section employs, as seen on the left part of Figure 6 in a similar fashion, thin sheet metal pieces to allow for taking up misalignment of the loading arm and allow the shear of the two yokes. The test-rig employs dead weights in order to load the bearing.

## 2.3. Measure wear

Wear is a, commonly unwanted, form of material removal. Measurement on journal bearings at Scania is done by calculating the volumetric difference from pre- and post-test measurement. These are carried out with a Coordinate Measurement Machine (CMM) which measures points on a geometrical object by touching it with a stylus, as seen in Figure 7.



*Figure 7. CMM measuring flatness of the bearing housing*

A CMM offers a very low level of uncertainty, depending on the distances measured. For short distances the uncertainty can be sub-microns. Given enough points a line or surface can be drawn. The bearing is measured on both sides several times, as to take tolerances of the piece and uncertainty of the CMM into account, This is done by tracing several lines in the radial direction of the surface, as seen in Figure 8.

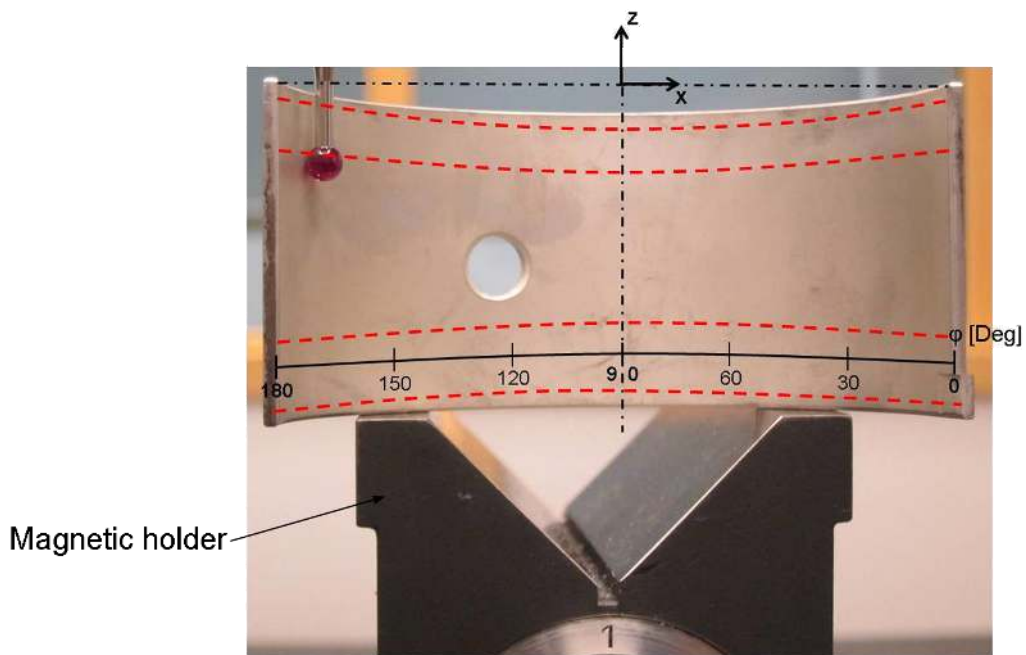


*Figure 8. How a bearing shell is secured and measured*

After measuring lines several times a filter is applied and the surface between the lines is interpolated. By subtracting the pre- and post-test measurement the volumetric wear can be calculated. This volumetric wear,  $V$ , is then set equal to the overlapping volume,  $V_c$ , in order to gain a reasonable wear depth, as seen in Figure 9.

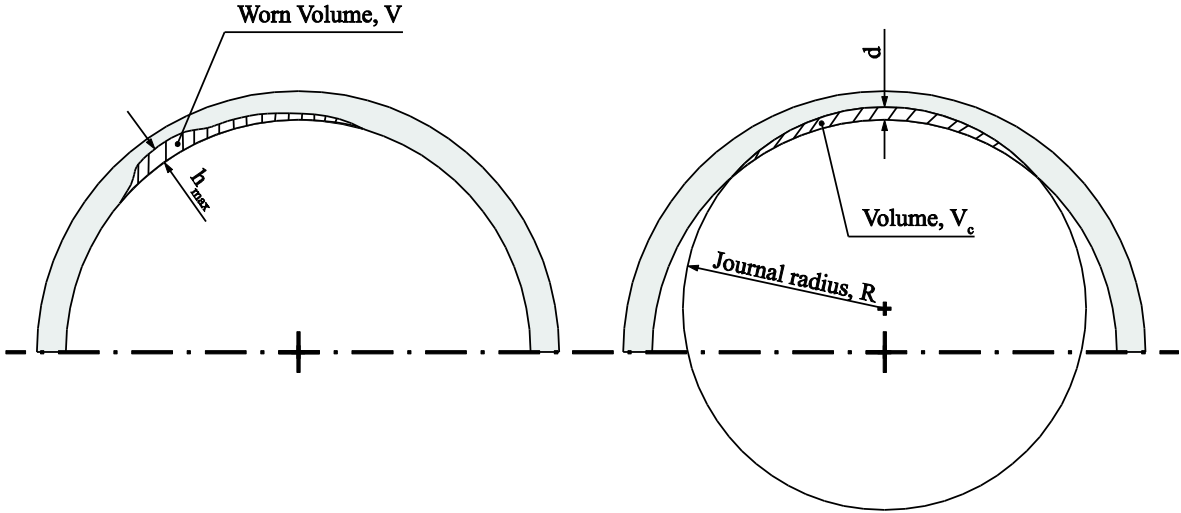


Figure 9. Worn bearing volume and overlapping volume

Both the wear volume,  $V$  and overlapping wear depth,  $d$ , are used for performance evaluation.

## 2.4. Safety

Interacting with a machine which has moving parts and high currents present is potentially dangerous. As such EN ISO 13849-1 exists for implementing a machine in a safe way. It breaks down the process of removing or mitigating risk into a workflow, as seen in Figure 10.

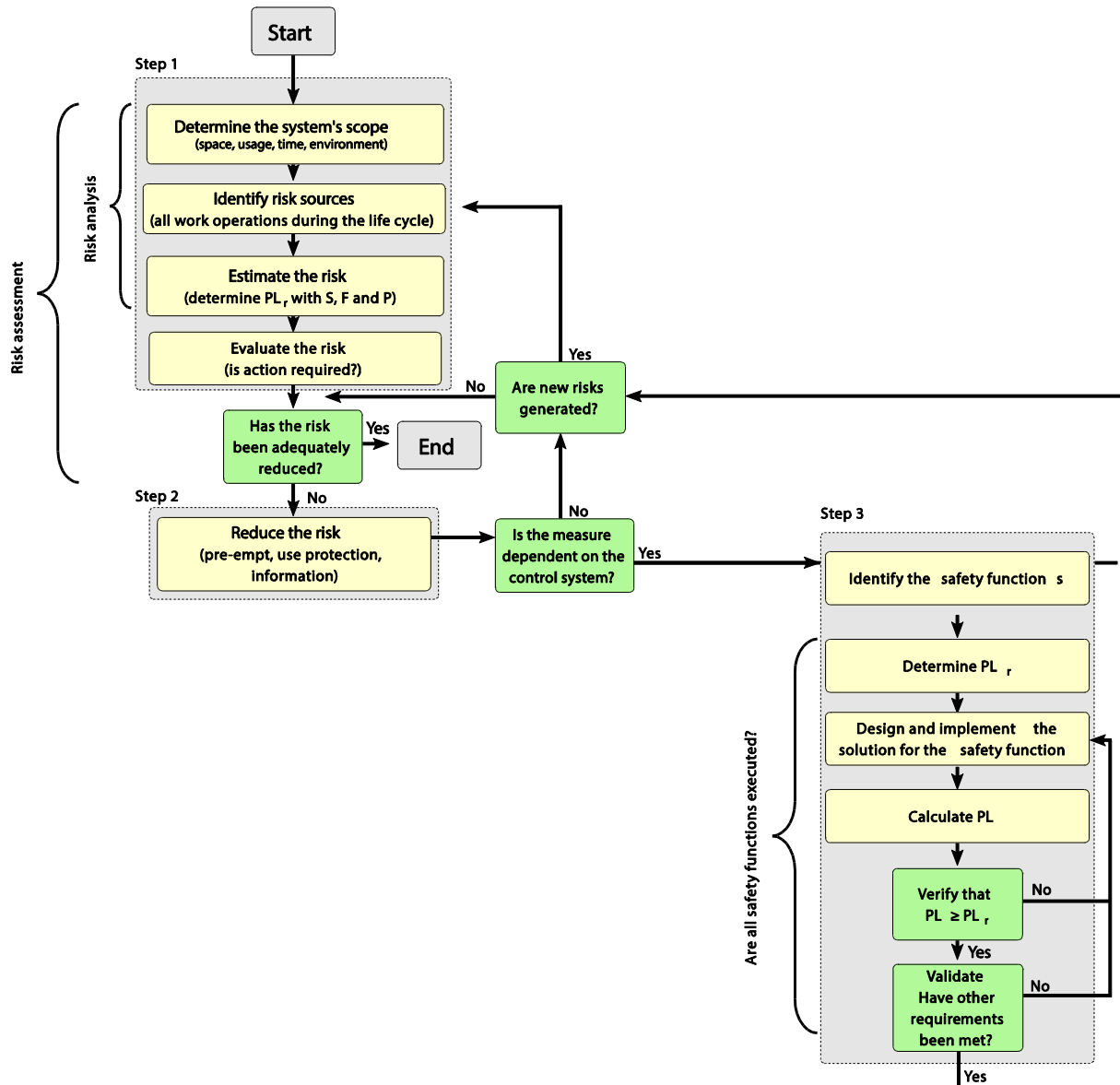


Figure 10. Flowchart for risk assessment and risk reduction (ABB AB Jokab Safety, 2011)

In order to make a risk assessment of a machine, a risk analysis of the system's scope is first performed. The space around the machine and the operational stages through the life time of the machine are taken into account. All work operations are then identified, broken down and assessed for risk. The risk is estimated using three factors: injury severity (S for severity), frequency of exposure (F for frequency) and ability of avoidance or limiting the injury (P for possibility). Each factor has two levels, which have no specified difference in the standard. Commonly they are interpreted as:

- S1 bruises, abrasions, puncture wounds and minor crushing injuries
- S2 skeletal injuries, amputation and death
- F1 less frequently than every two weeks
- F2 more often than every two weeks
- P1 slow machine movements, plenty of space, low power
- P2 quick machine movements, crowded, high power.

By following the tree structure in Figure 11 you gain a risk-estimation for your risk sources.

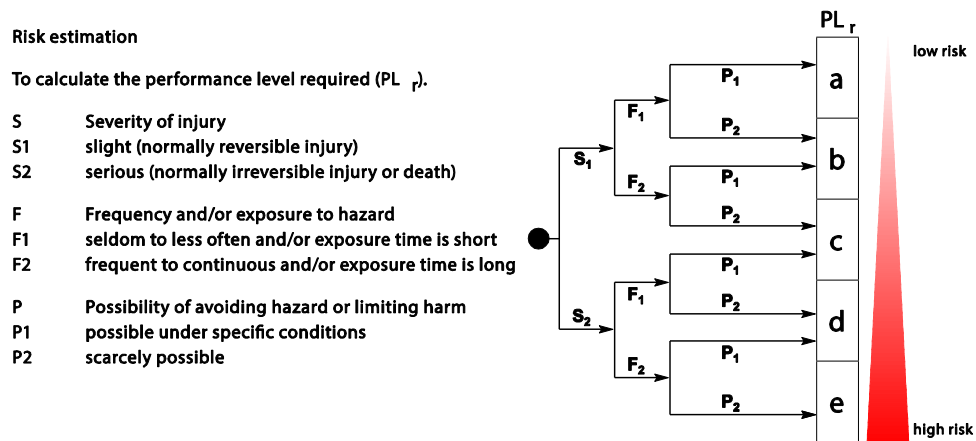


Figure 11. Risk estimation flowchart (ABB AB Jokab Safety, 2011)

Once this is done the risks are benchmarked against the required Performance Level ( $PL_R$ ) that is deemed acceptable. If there is a need to reduce the risk for a task, step 2 and possibly step 3 in Figure 10 are taken in order to reach an acceptable risk level. Step 3 is commonly electronic and performed by an electrical or mechatronics engineer. Relays, switches, emergency stop buttons and other components in a safety function are commonly rated at different Performance Levels, making it straight forward to implement a safety function.

## 2.5. Electrical noise

Data acquisition of voltage, temperature, pressure and strain measurements is an important part in an industrial environment. These environments often include hazardous voltages, transient states and fluctuating ground potentials that can damage measurement instruments or ruin measurement accuracy (National Instruments, 2014). Common ways this can happen is due to electromagnetic interference (EMI) or lack of electromagnetic compatibility (EMC) with surrounding electronics. EMI can be caused by two principal ways; either by conduction or by radiation (EMR). Conduction means that the interference is coming from an input cable, for example via the power cord and into a computer. The power cord then not only carries a clean 230 VAC sinusoidal signal, but also overlaid noise to this signal which propagates inside the computer which for example may cause a connected stereo to audibly hum. Radiation on the other hand bridges air in order to transmit the energy of the noise, such as via

FM-waves or microwaves. Radiation may originate from cables or wires acting as an antenna and nearby cables or wires may then pick this radiation, see Figure 12. Magnetic fields are induced by a change of current in a cable.

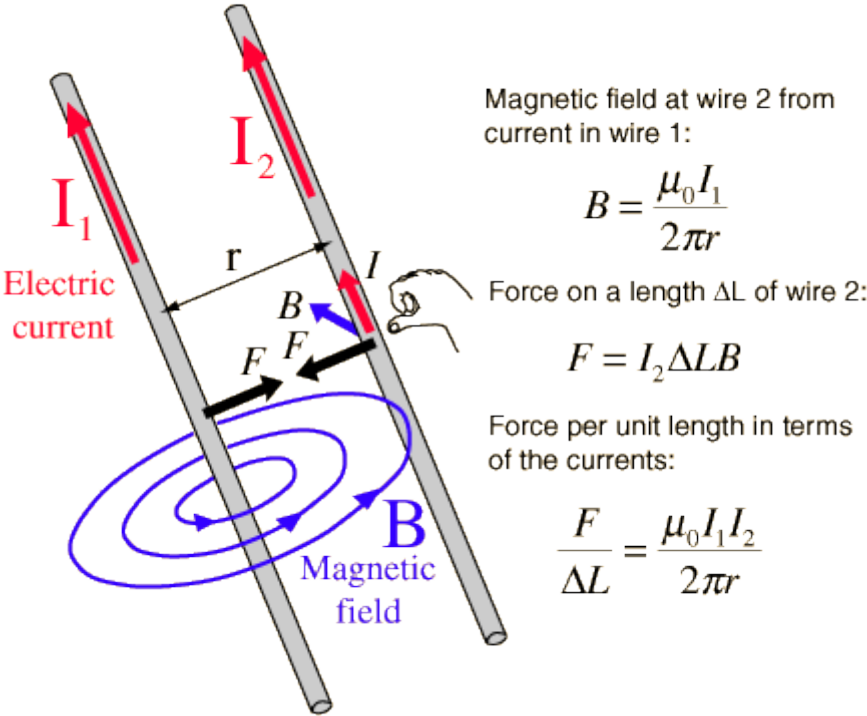


Figure 12. Magnetic field induced in wire 2 by wire 1 (Nave, 1997)

Noise propagated between wires in a cable is commonly referred as crosstalk, as seen in Figure 13.

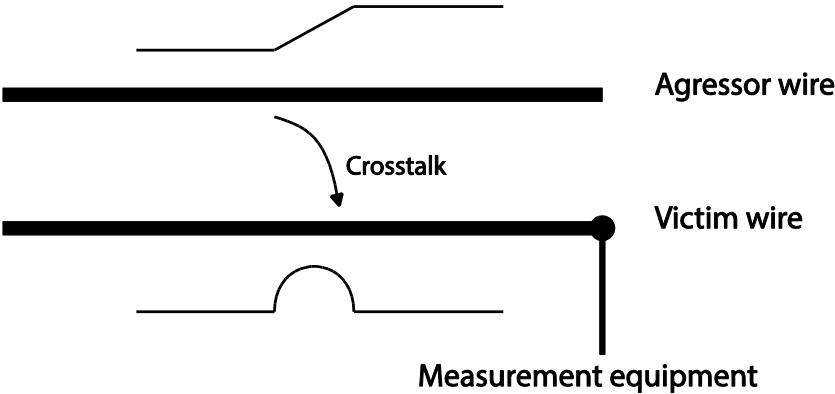


Figure 13. Example of crosstalk in a cable between wires.

A common way to deal with noise is to implement shielding on sensitive and noisy cable as well as shielding the components they connect to. The cables and exterior of electrical components in essence act like Faraday cages, as seen in Figure 14.

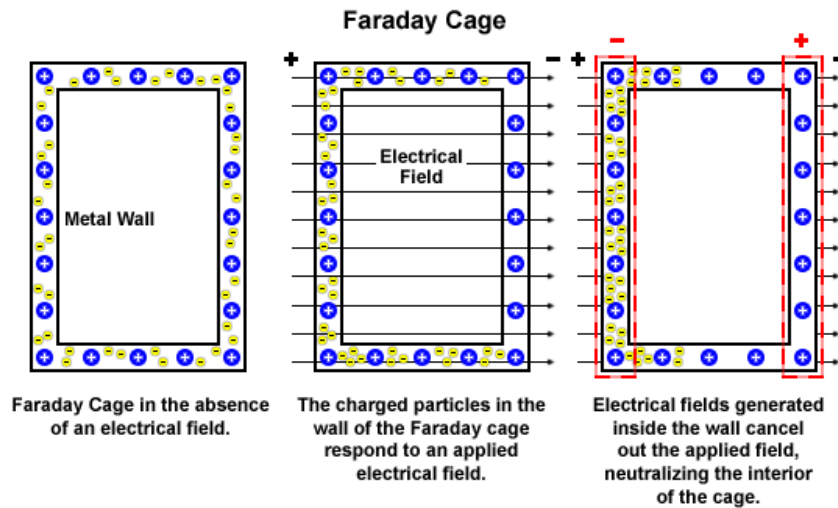


Figure 14. Faraday cage (National High Magnetic Field Laborator, 2014)

An example of a Faraday cage is the microwave oven. These commonly have windows with meshed nets, but which act as a Faraday cage even though it allows for looking at the food. This works by sizing the holes in relation to the frequency which is to be blocked, thus blocking the microwaves, but allowing light to pass. All items in a system need to be properly grounded in order to bleed of charges that could otherwise build up and damage components or a user.

Cables are commonly shielded with thinner material than casings and as such are more susceptible to noise. In order to assert a good shield the grounding of the cable is important. While a solid shield theoretically offers the best noise reduction, most cables have a braided shield, as it is much simpler to manufacture (Dataforth, 2002). Should extra shielding be needed, braids are available separately, allowing for extra protection.

### 3. PREVIOUS WORK

---

*In this chapter the work that has previously been carried out is presented.*

The test-rig developed during the AMD-course was designed with requirements drawn up in cooperation between the team and Scania; these are listed in Appendix A. A CAD-model, as seen in Figure 15, was continuously improved and detailed.

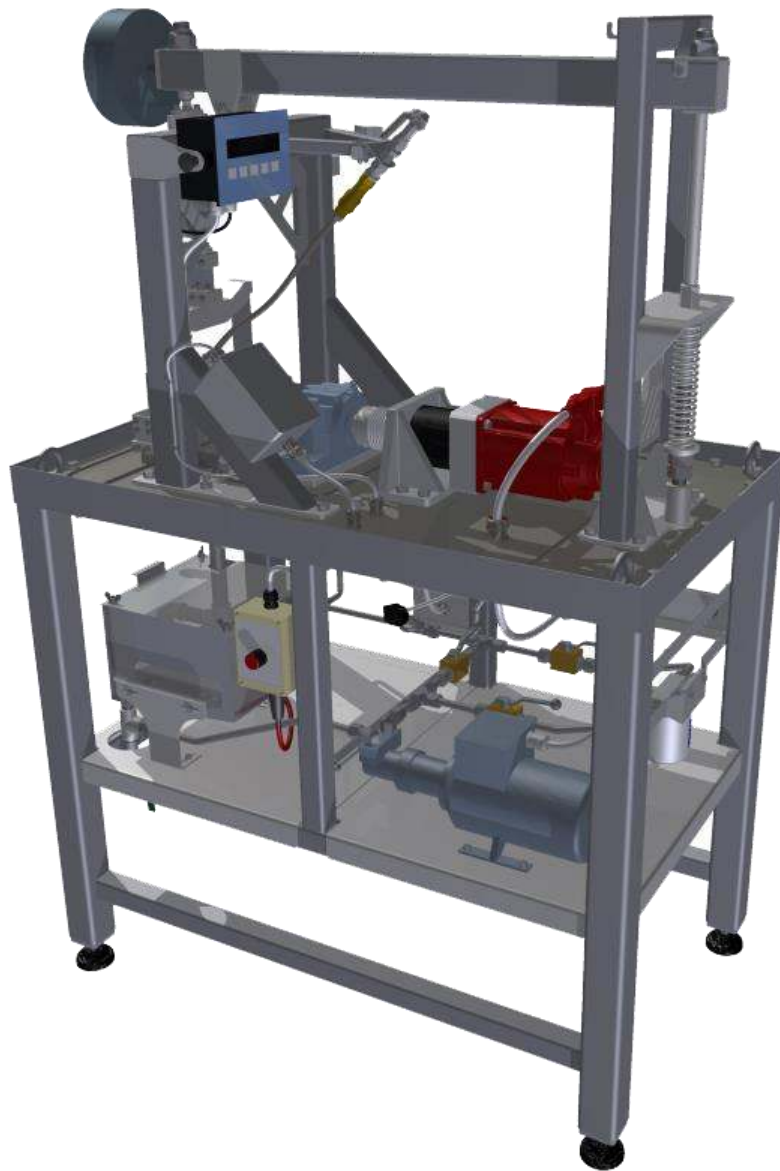


*Figure 15. The DM5k*

The test-rigs requirements are listed in Table 1.

Table 1. Test-rig requirements

Speed (rpm)	0 - 1,000
Acceleration (rad/s <sup>2</sup> )	0 - 210
Oil temperature (°C)	ambient - 150
Oil pressure (bar(g))	0 - 5
Radial loading (N)	0 - 5,000

The test-rig can be broken down to four major sub systems.

1. Main structure, as seen in Figure 16.
2. Power train, as seen in Figure 17.
3. Loading mechanism, as seen in Figure 18.
4. Oil system, as seen in Figure 19, Figure 20 and Figure 21.

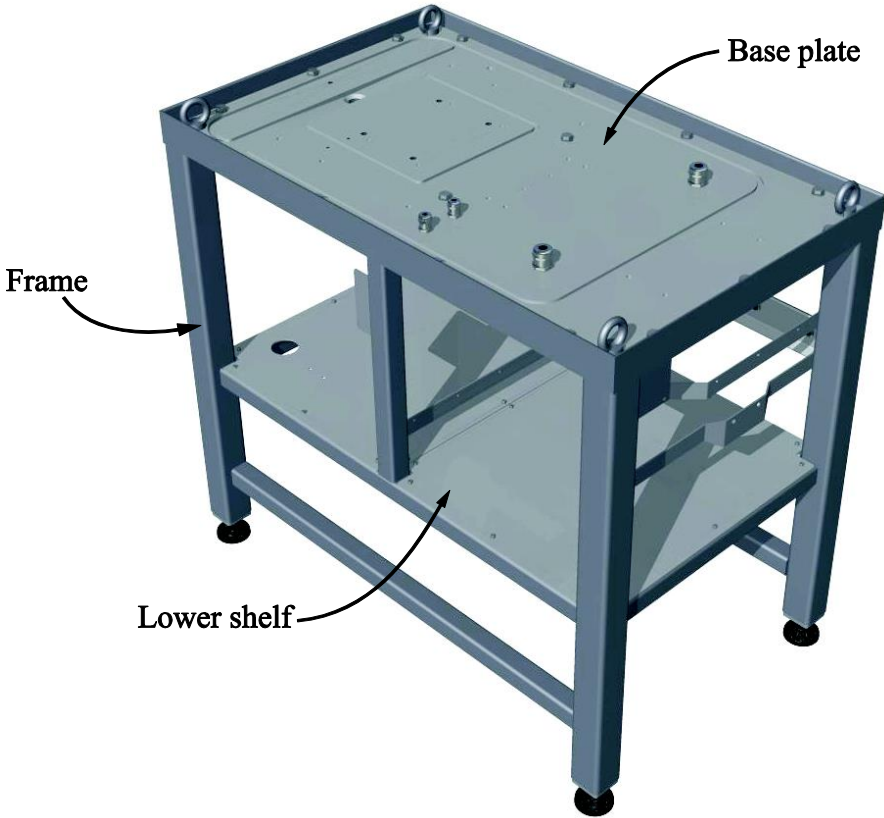


Figure 16. Main structure

The main structure includes square profiles between the legs which allows for the rig to be moved with a pallet jack.

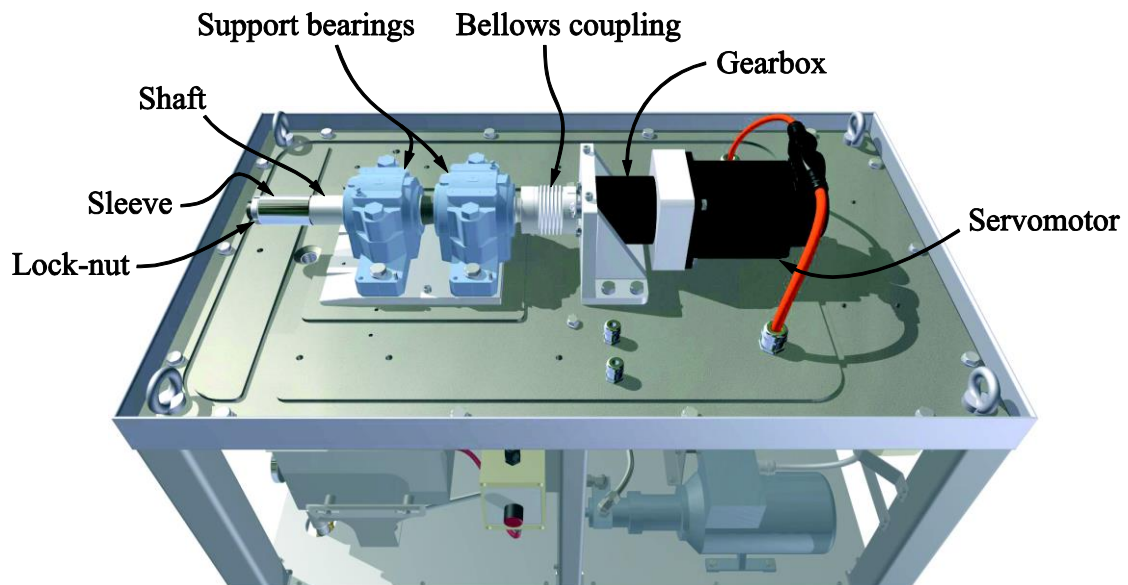


Figure 17. Power train

The powertrain uses guiding pins, which connect to the baseplate, in order to align all components.

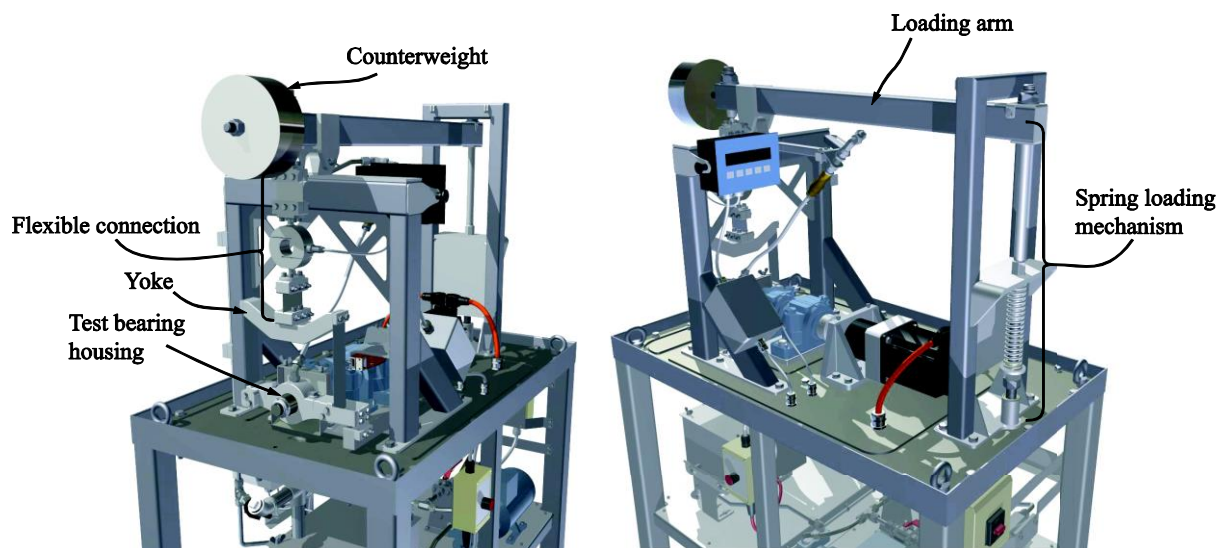
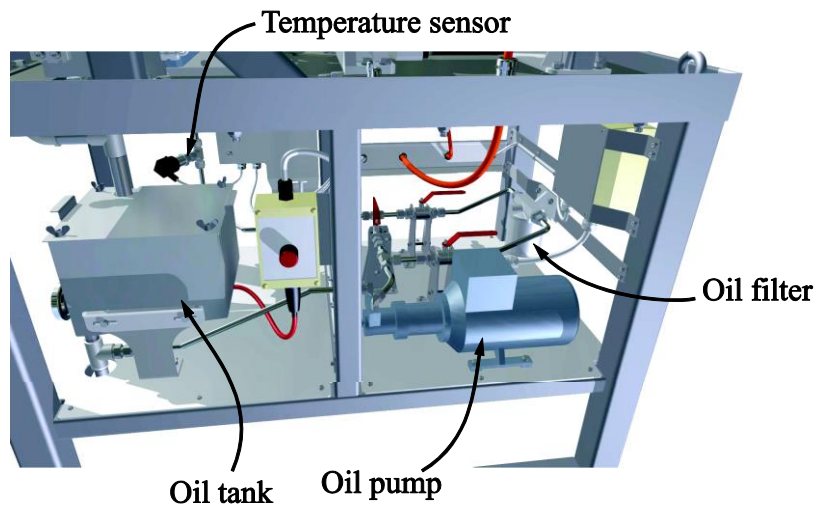


Figure 18. Loading mechanism

The loading mechanism allows for easy loading of the test-bearing by compressing a spring with a wrench.



*Figure 19. Oil cycle as seen from the front*

The oil tank features a heating mat which is set manually. The layout was designed so that all features would be easily accessible.

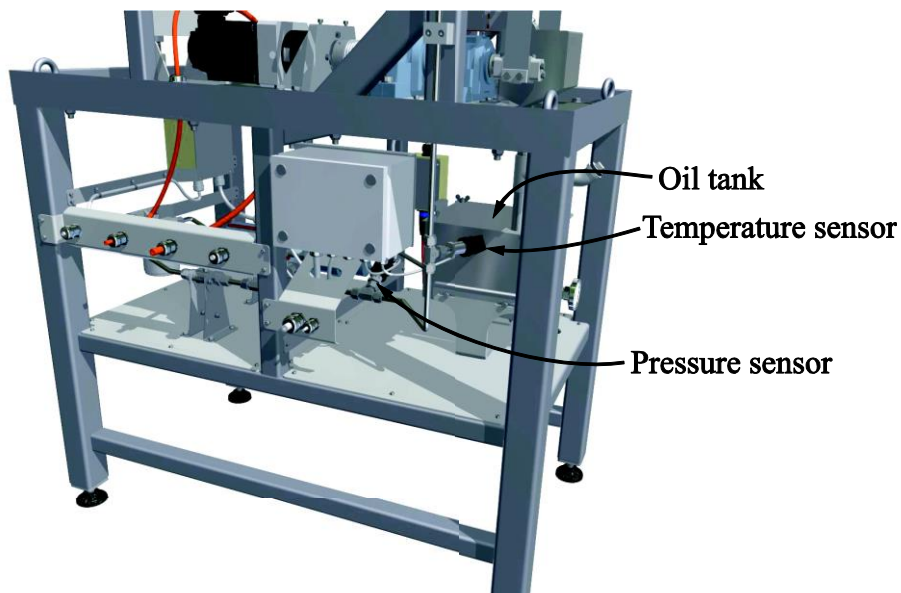


*Figure 20. Oil cycle as seen from the rear*

All sensors on the rig feature current-based signal in order to reduce risk of noise.

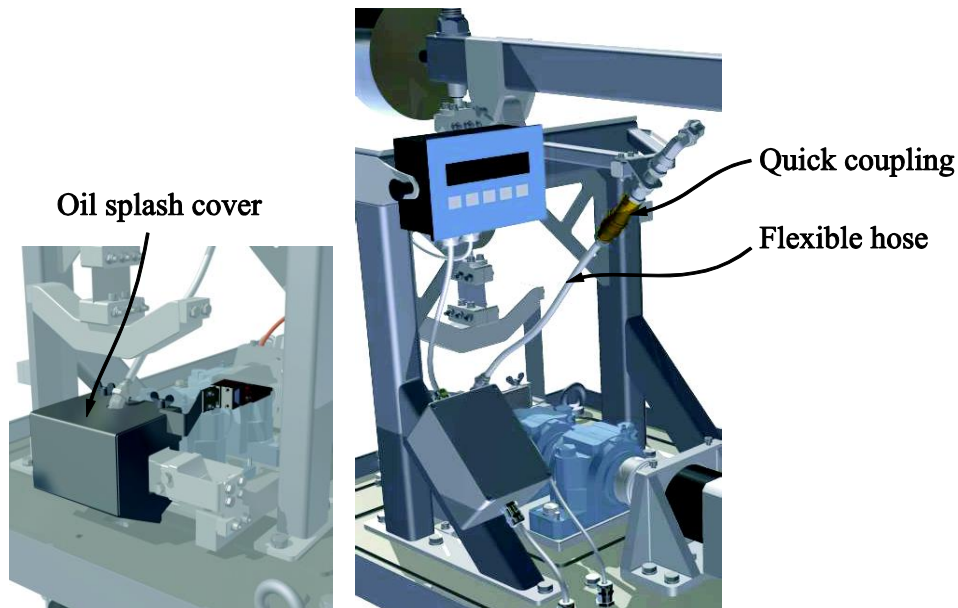


Figure 21. Oil cycle components on the top of the rig

### **3.1. General test-rig description**

The test-rig gives the operator the ability to adjust certain parameters before starting a test. These parameters are:

- Shaft speed
- Acceleration and deceleration
- Durations at standstill and running speed
- Number of cycles to run
- Load applied to test-bearing
- Oil temperature
- Oil pressure

In addition to setting these parameters, the user selects the size of the journal by choosing a suitable sleeve, allowing for different clearances to be evaluated as well.

All listed parameters, except the loading and oil temperature are set in software on the computer which is connected to the test-rig. To change test-bearings the upper yoke, test-bearing housing and sleeve are removed as a unit with the removal of four screws, as can be seen in Figure 22.

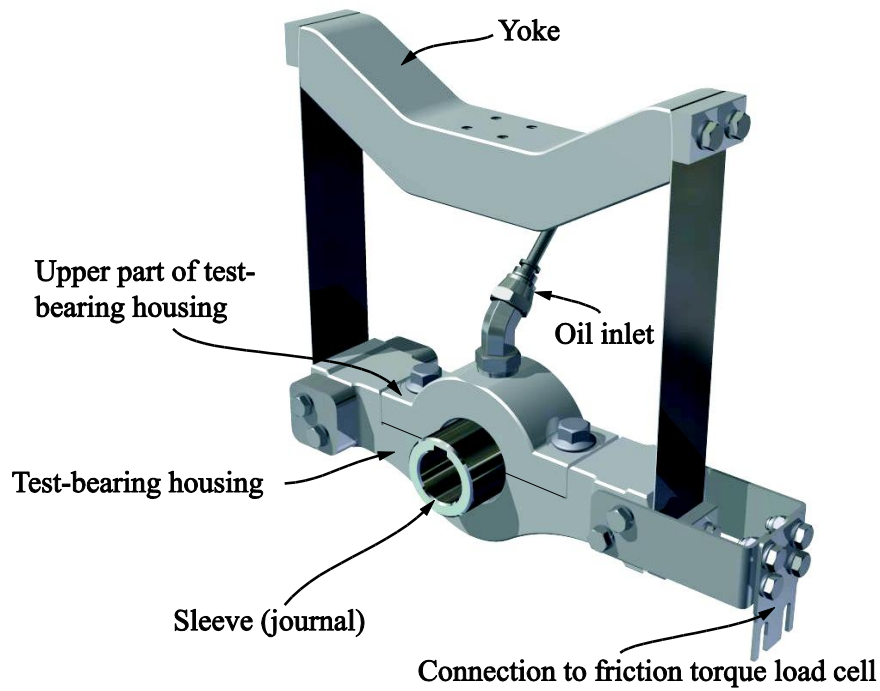


*Figure 22. The bearing-housing assembly*

The upper part of the test-bearing housing is removed and the sleeve lifted out, in order to reduce the risk of damaging the tested bearing shell surfaces. Then the tested bearing shells are removed and new ones pressed into the upper and lower part of the housing, as seen in Figure 23.

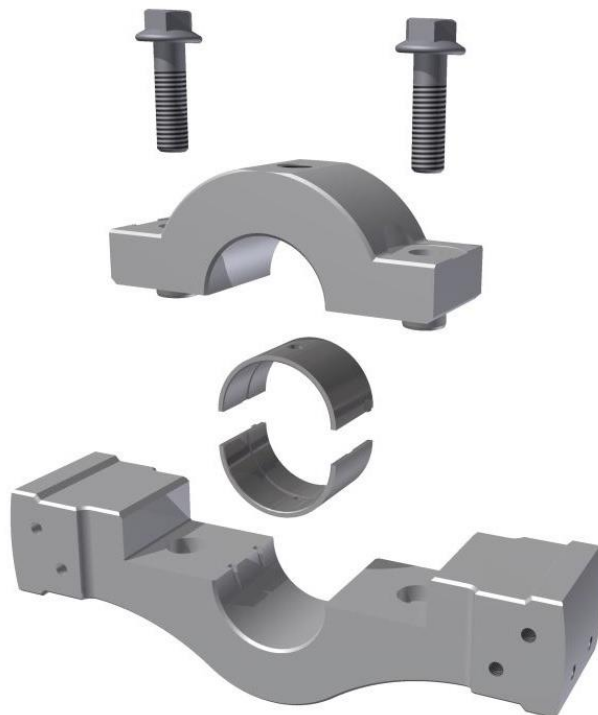


*Figure 23. Lower and upper part of test-bearing housing*

Thereafter the sleeve is added and bearing-housing is assembled. After connecting the yoke to the flexible connection and installing the splash cover the system can be loaded.

The friction torque is measured with a load cell, as seen in Figure 24, in a similar fashion as the Eindhoven concept.

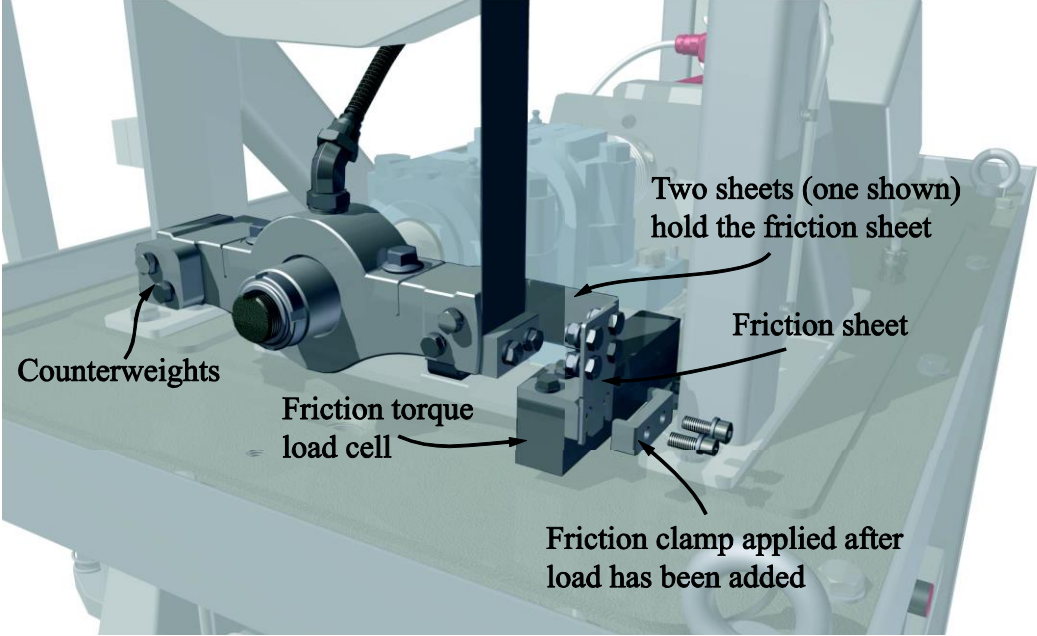


Figure 24. Friction measurement implementation

The shearing of the structure is allowed with thin sheets, clamped together with friction clamps, as seen in Figure 25.

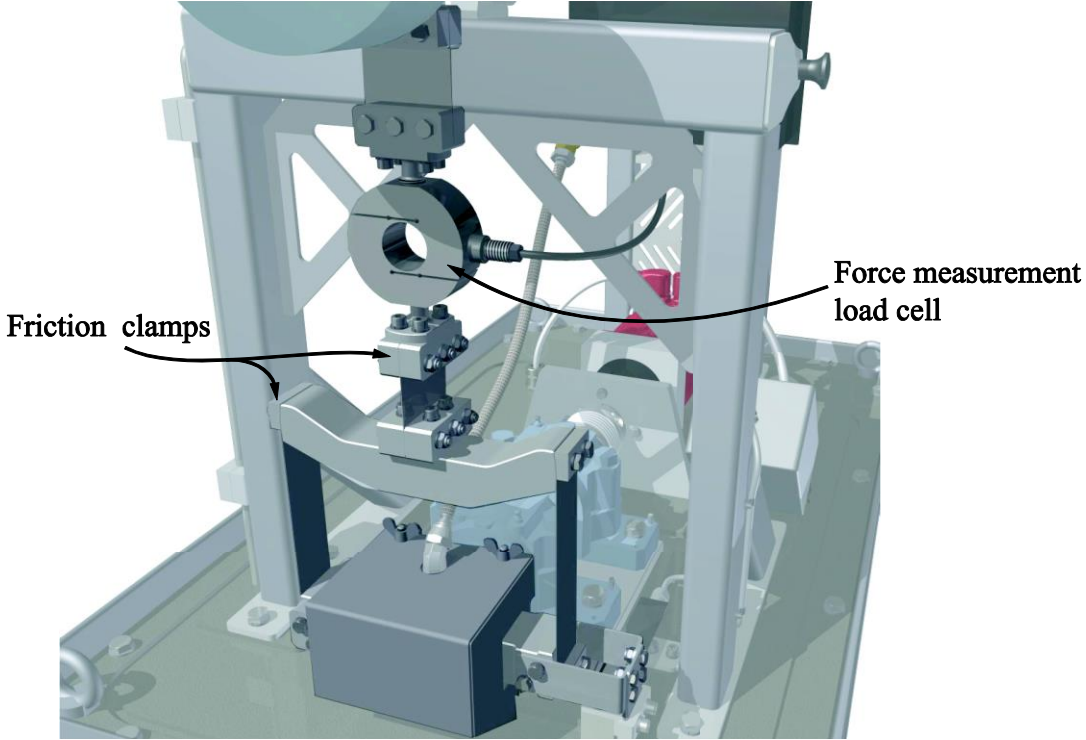


Figure 25. Flexible connection between test-bearing housing and loading arm

Furthermore the two sheets below and above the load cell, as seen in Figure 25, allow for some misalignment. In total three degrees of freedom are allowed by the structure. The load cell is connected to a display so the user instantly can see how much force is applied to the bearing, without having to look at the computer. The loading itself is done by turning the nut on the partly threaded rod, as seen in Figure 26. This compresses the spring, forcing the loading arm to be pulled downwards, in turn pulling on the test-bearing housing.

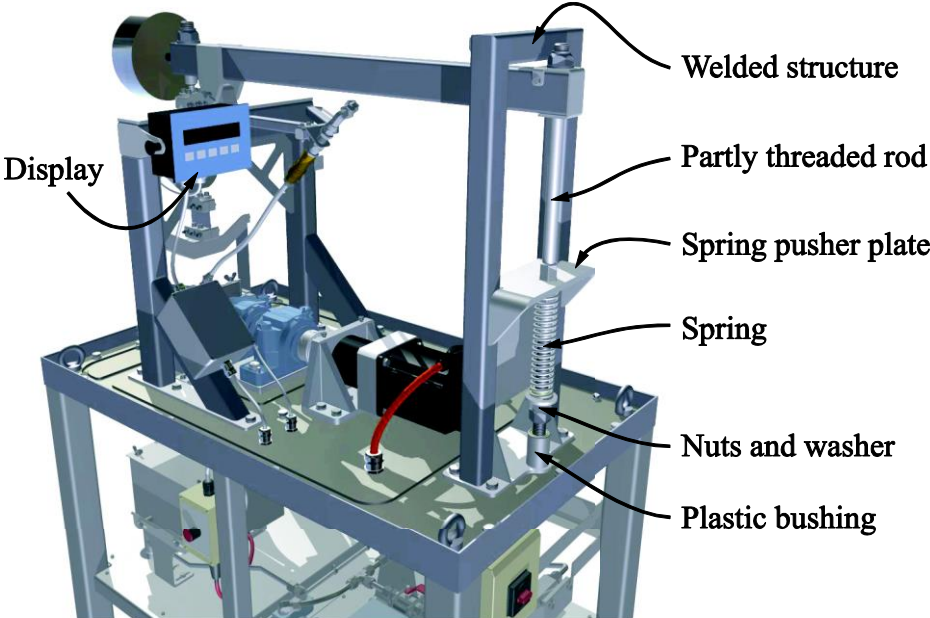


Figure 26. Parts of the loading mechanism

The welded structure protrudes over the loading arm, in order to secure the loading arm in the case of a catastrophic failure. On the end of the loading arm sits a counterweight, which can be adjusted in order for the unloaded system to not apply any force on the shaft. This allows easy removal of the test-bearing housing and upper yoke.

On the lower shelf of the test-rig are the main components of the oil supply system as well as most electrical wiring.

The oil tank is positioned under the bearing housing so the lubrication oil that exits the bearing housing drips through the base plate in the frame and to the tank. Underneath the tank is a heating mat that is connected to a manual temperature dial which can be seen in Figure 27.

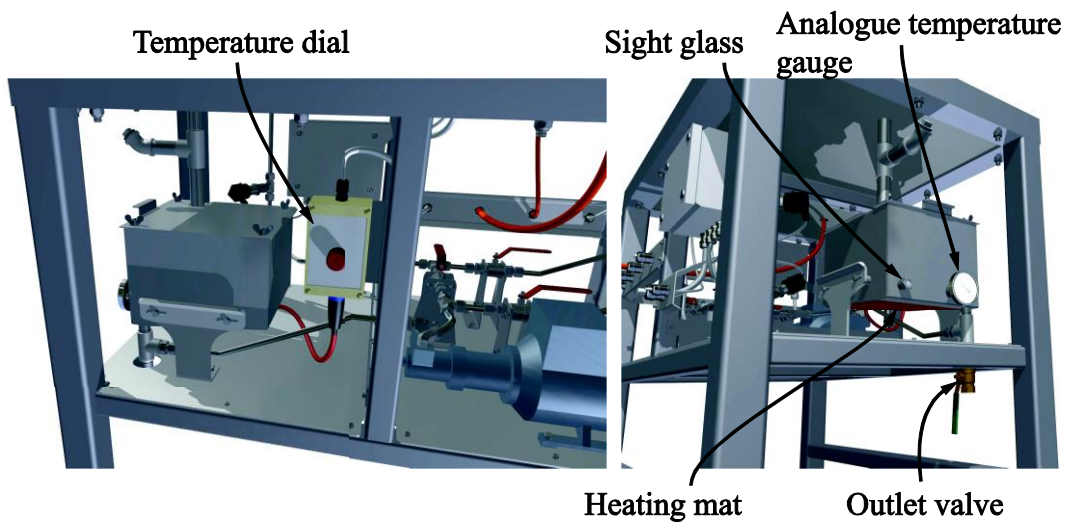


Figure 27. Heating and oil details

The oil temperature cannot be changed during operation. On the oil tank is a sight glass, allowing the user to see the oil level as well as an analogue temperature gauge. Underneath the oil tank an outlet port allows for draining the oil tank.

On the pressurised side of the oil system the user has the possibility to route the oil through an oil filter or by bypassing it with adjusting valves, as seen in Figure 28.

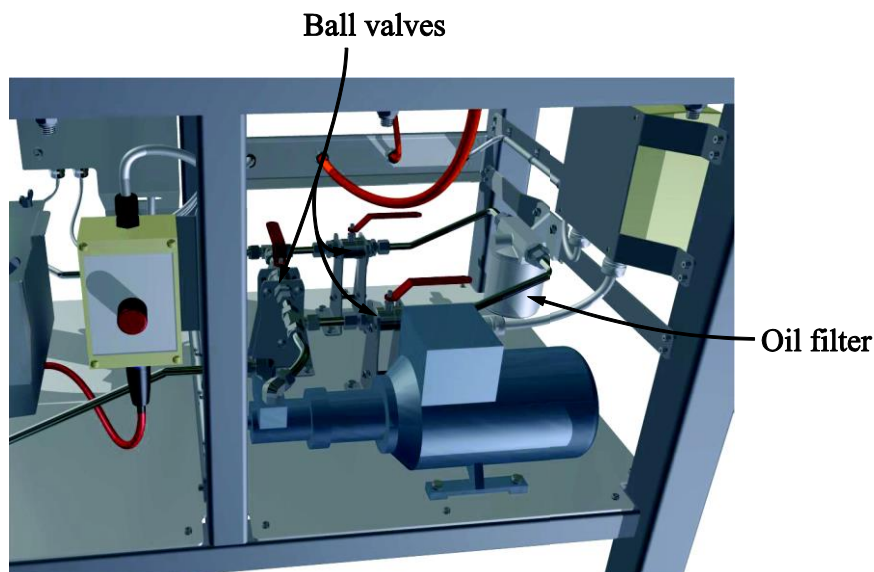


Figure 28. Routing of the oil through oil filter or directly fed to test-bearing

After the bypass loop are two sensors which send temperature and pressure values of the oil to the computer. The temperature data is only logged, as the temperature is not adjustable from the computer.

After the temperature sensor the lubrication pipe goes through the base plate and to the top of the load frame subassembly. From there a flexible hose is used to attach the oil supply line to the test-bearing housing while introducing as little interference as possible to the friction measurement. A quick coupling allows easy engagement and disengagement by hand when

working with the test-bearing housing. The supplied oil to the test-bearing escapes as side leakage, but due to safety reasons and to secure that the oil stays in the cycle an oil splash cover is fitted around the test-bearing housing. This cover guides the oil to the grooves in the base plate which furthermore guides the oil towards the pipe leading back into the oil tank.

### ***3.2. The test cell***

Initially a mobile rig was discussed; with a wish for a simple three phase power plug to install the test-rig at a location. As the project progressed, the size of the rig had grown and issues with safety made it more suitable to be placed in a test cell. A test cell was selected at KTH for installation which features a window and space outside for the computer.

### ***3.3. Status at end of Advanced Machine Design course***

At the end of the AMD-course a complete CAD-model and detailed drawings of the test-rig was delivered. A few components, such as shaft, test-bearing housing and yoke had been manufactured, but a majority of components were deferred due to Christmas and increased end-of-the-year manufacturing delivery times.

## 4. CHANGES AND IMPLEMENTATION

---

*In this chapter the body of changes, implementations, changes and assembly are presented.*

While much work was done during the AMD-course, many finer details of the test-rig were evaluated during this thesis.

### **4.1. Electrical cabinet**

During the later stages of the AMD-course, when the servomotor had been chosen, the need for an electrical cabinet became apparent. The electrical cabinet was procured after a thorough procurement procedure, with five companies contacted and four delivering a quote. The thesis was to a large extent two projects which progressed in parallel. Responsibility was split for the electrical domain and mechanical domain. The specifics of electrical cabinet were discussed with the contractor and Mikael Källberg, an electrical engineer, as the detailed knowledge for electrical systems was not within our knowledge domain.

### **4.2. Risk Assessment**

During the AMD-course safety and usability was of a major concern. The largest risks may have been obvious, such as hot oil and a rotating shaft, but to better understand and formally manage the risks, a risk assessment, as described in chapter 2.4, was done.

The risk assessment starts with defining the scope and the user interactions with the machine.

The machine is situated in a test cell, accompanied with an electrical cabinet. Outside the test cell a computer is situated, which is used to control the test-rig.

There are three main steps that the operator needs to execute in order to run tests. Firstly the evaluating test-bearings need to be installed. This is accomplished in an unloaded system. In order to run a test the system needs to be pre-loaded. This is accomplished by turning a nut with a wrench, in turn compressing a spring and pulling, via a loading arm on the test-bearing. The test is then run, which spins a shaft at various speeds and pumps oil at a pre-set temperature and pressure into the test bearing. After a test, the system is unloaded in the same manner as it was pre-loaded and the bearing shells extracted. No work should be necessary in the test cell during testing. Any errors to the machine are handled in an offline-setting, where power is cut to motors and the system is unloaded. The system is run in a test cell with the door closed.

The machine is deemed to be running full time at one week periods with downtime of three days in between. It is deemed to be running only during school semesters (2x20 weeks per year). This gives an uptime of 70 % during semesters and 196 days per year of running time. It is considered that an error during any phase of testing will cause the testing to be invalid and give allowance to a three days downtime as a result. It is assumed that there will be a maximum one error per every five test cycles run. The maximum number of cycles for

protection function machine is thus  $196 \text{ days/year} \cdot 1 \text{ cycles} / 7 \text{ days} + 20 \% \text{ failure rate} = 34 \text{ cycles/year}$  (F1).

It is considered that if the machine would unexpectedly start the shaft the operator would be at risk for severe injury (S2) and would not have time to move away from the machine in due time (P2). The protective feature needed to access the machine is deemed to be  $PL_r=d(S2,F1,P2)$

It is considered that if the machine would unexpectedly start the pump and spew hot oil the operator would be at risk for severe injury (S2) and would not have time to move away from the machine in due time (P2). The protective feature needed to access the machine is deemed to be  $PL_r=d(S2,F1,P2)$

It is considered that if the machines loading mechanism would unexpectedly break that the operator would be at risk for severe injury (S2) and would not have time to move away from the machine in due time (P2). The protective feature needed to access the machine is deemed to be  $PL_r=d(S2,F1,P2)$ .

### **4.3. Safety-measures**

In order to address these risks, safety measures were evaluated and implemented.

#### **4.3.1. Door breakers**

The doors into the test cell are fitted with redundant breakers, which cause an emergency stop of all high voltage electrical systems in the test cell, causing both the oil system and shaft to stop.

#### **4.3.2. Safety cover**

The rotating shaft was enclosed with a steel cover with a thickness of 1.5 mm, as seen in Figure 29.

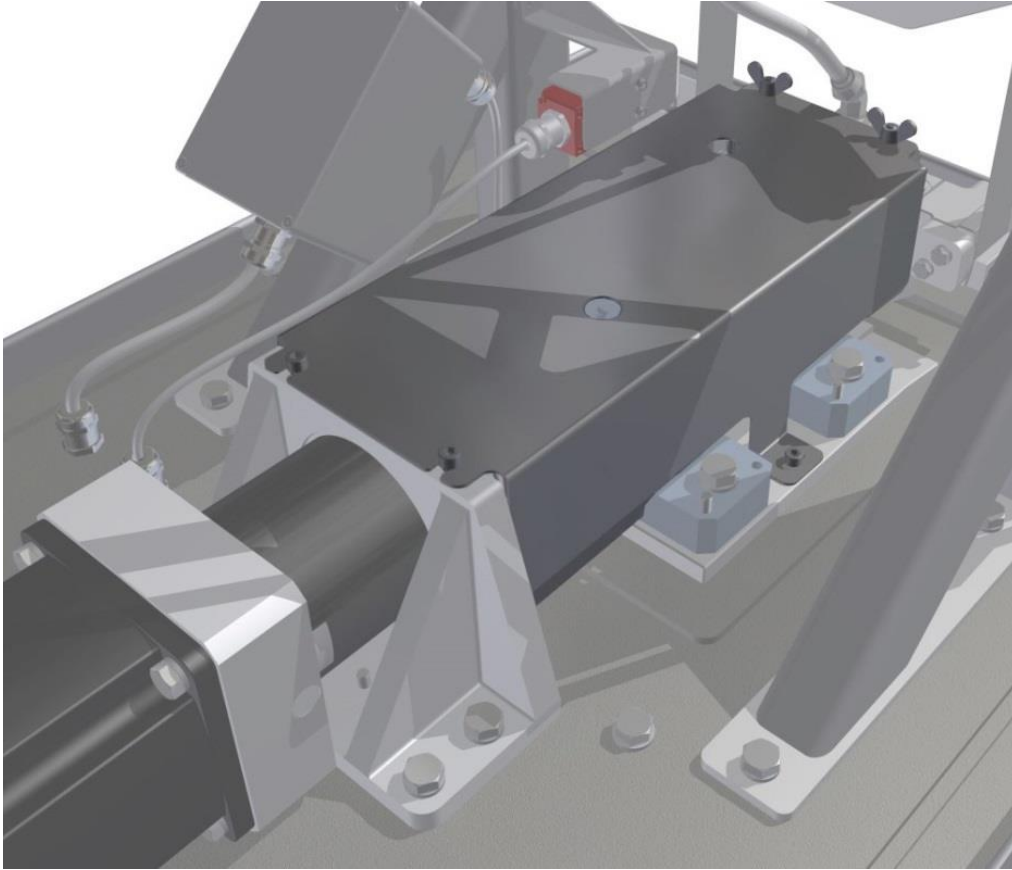


*Figure 29. Safety cover*

It is bolted down with four M6 bolts. The cover will reduce the risk of a user can come in contact with the rotating shaft and furthermore act as a containment from broken parts in case of a catastrophic failure. It is worth noting that a user should not be able to be in the room with a running shaft due to the door breakers installed.

#### **4.3.3. Splash cover breaker**

The same type of breaker as used for the doors is also fitted to the oil splash cover. Starting the rig would allow hot oil to spew onto the user or get tangled with the spinning shaft. If the user is working on the test-rig with closed doors, it is not possible for a malicious user to start the rig if this cover is removed. The splash cover is necessary to remove in order to do any meaningful work on the test-bearing.

#### **4.3.4. Pump breaker**

In order to allow maintenance on the oil pump, a breaker was installed. This is a risk that was not identified in the risk assessment, but which was pointed out as a necessary feature by the firm designing the electrical cabinet.

#### **4.3.5. Insulation**

Most parts of the test rig that are in contact with the oil system are insulated via glass fibre and aluminium foil, in order to reduce burn risks, as seen in Figure 30. The insulation was

however not possible to fit for the test-bearing housing or flexible hose, and a user needs to demonstrate special precautions when working around these parts.

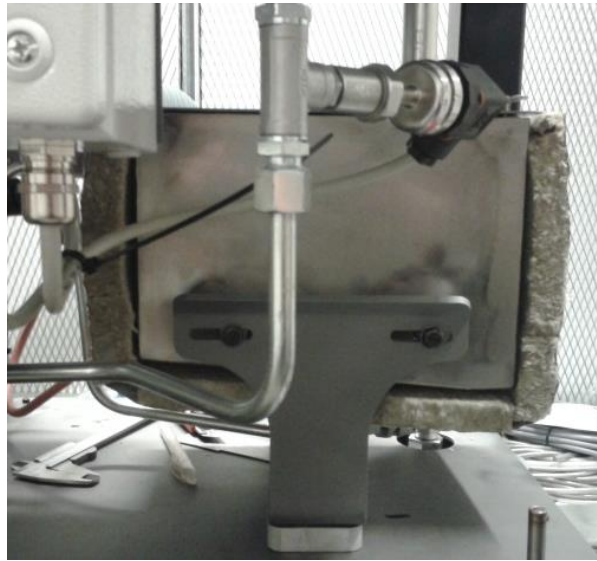


*Figure 30. Insulation of the oil tank*

#### **4.3.6. Loaded spring**

During the AMD-course this was identified as a possibly dangerous part and was designed with this in mind.

#### **4.3.7. Emergency stop buttons**

An important factor to hindering injury to person or damage to equipment is well placed emergency stop buttons. One button close to the test-rig one button was placed on the electrical cabinet while one was placed outside the test-cell, as seen on Figure 31.

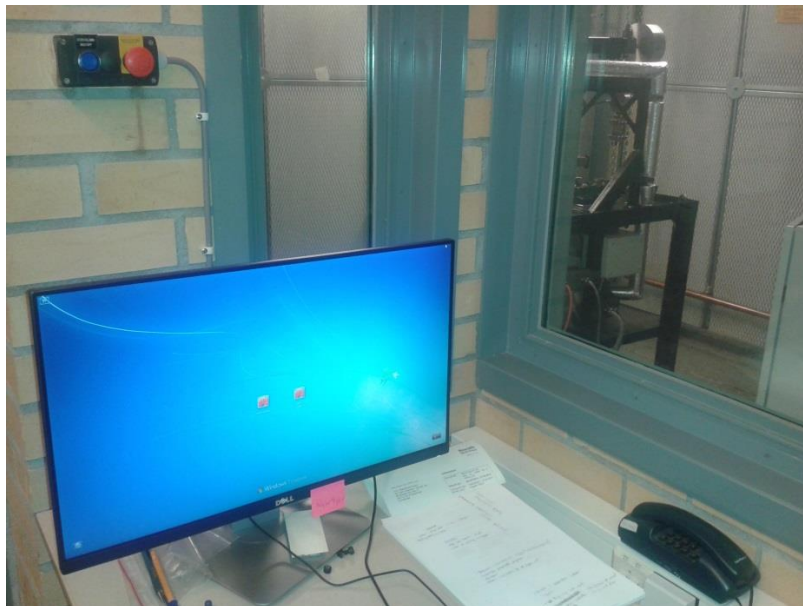


*Figure 31. Computer setup with window to test-cell*

## 4.4. Assembly

### 4.4.1. Process

The first task during the thesis was to divide the manufacturing of remaining parts between Scania's workshop and KTH workshop to optimise delivery time. Dynamate, a subsidiary to Scania, was used to manufacture parts that required high tolerances.

### 4.4.2. Assembly of power train

At the midpoint of the thesis, key parts such as the frame and base plate were delivered, enabling us to start assembling the test-rig. First the main structure was assembled, and then the power train was assembled. Good alignment between the support bearings and motor support bracket was achieved by using guide pins. The shaft features a shoulderless design, with adaptor sleeves between the shaft and bearing, as seen in Figure 32.

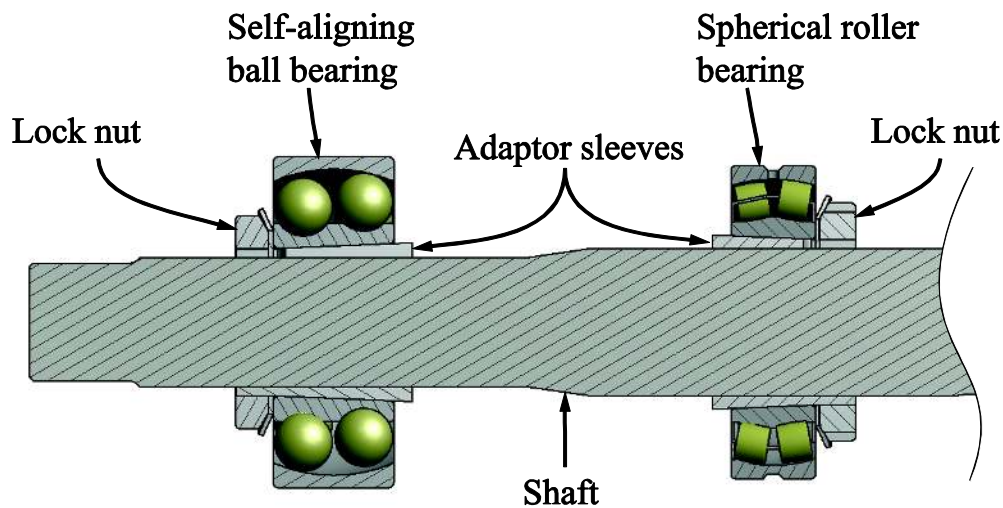


Figure 32. Simplified cross section of shaft and support bearings

The bearings are housed in pre-built bearing housings. When assembling the bearings, it became apparent that way of the axial positioning of the bearings was unsatisfactory. Attempting to tighten the lock nut resulted in the bearing sliding in both axial and radial direction, as there was no shoulder to push the adaptor sleeve against or any radial locking, as seen in Figure 33.

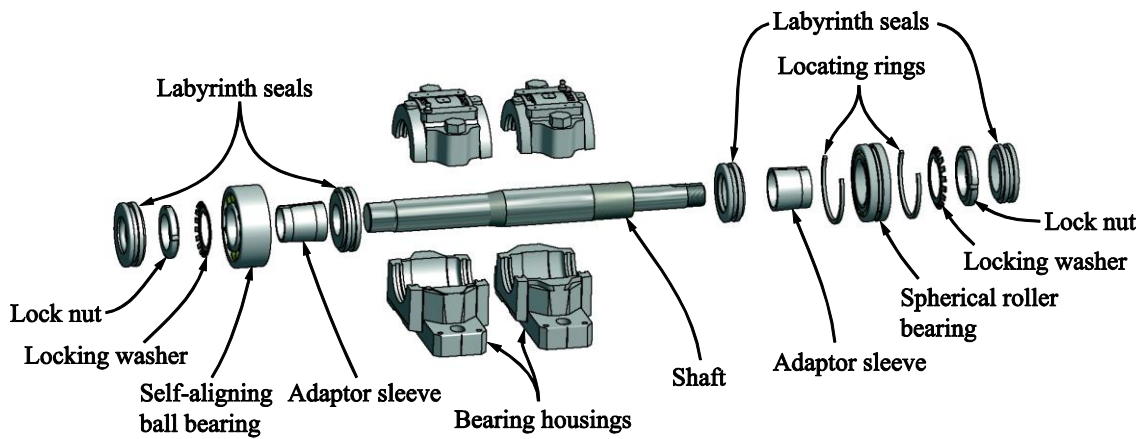


Figure 33. Exploded view of shaft and bearings

A shaft clamp, acting as a temporary shoulder and rotational lock was designed and manufactured, as seen in Figure 34, to remedy this problem.

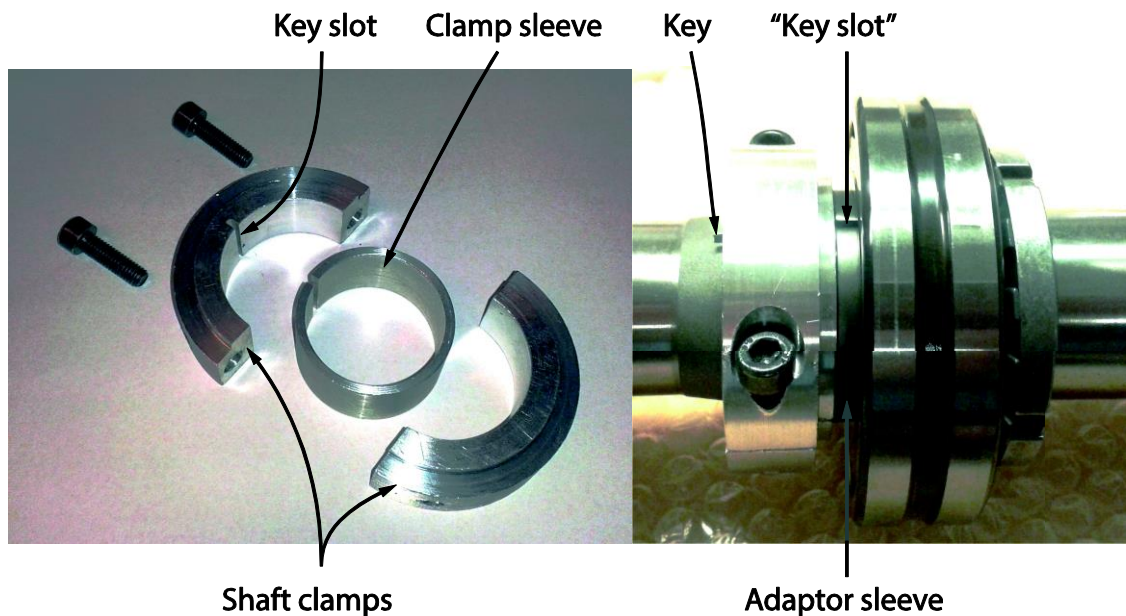
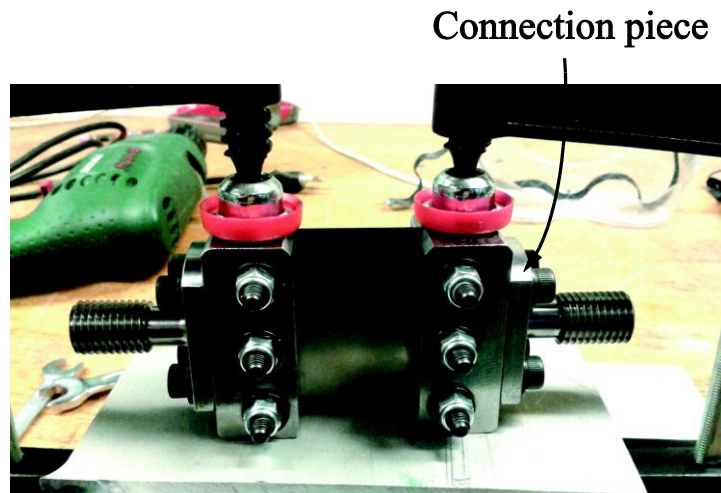


Figure 34. Exploded view of shaft clamp and in use

By accounting for the width of the bearing and its position on the adaptor sleeve the mounting distance from the end of the shaft was calculated for the shaft clamp. An adaptor was manufactured to allow fit it to both bearings. A key was inserted between the shaft clamp and adaptor sleeve to lock in rotational direction. After the support bearings had been fastened, the shaft and bearings were placed in their bearing housings and the coupling, motor support bracket, gearbox and motor were mounted.

#### 4.4.3. Assembly of loading mechanism

The load frame, spring frame and loading arm were mounted to the base plate, while the flexible connection, as seen in Figure 18, was put together in steps with each pair sheet clamp sub-assembled, as seen in Figure 35. These were measured for straightness and concentricity in a lathe by clamping steel spacer between the clamps in order to gain rigidity.



*Figure 35. Mounting friction clamps*

The lathe was spun by hand, while an indicator clock was used to measure the run-out. The position of the connection piece was then adjusted until it was assessed that a better result could not be attained. The test-bearing housing and yoke were positioned on a flat surface and the sheet metal pieces clamped together.

#### 4.4.4. Assuring mechanical repeatability

One of the priorities for the test rig is to be able to run repeatable tests. The test-rig however has many parts and numerous connections, which add uncertainty to the repeatability, as connections in a loaded or vibrating system move over time.

In order to provide as good repeatability as possible, the user is obligated to follow a step-by-step instruction, with information on tightening torques prior to running a test. These instructions are available in a user manual, which has been prepared for the test-rig.

The yoke is disassembled and reassembled with the friction clamp with every test, as described by Figure 36.



*Figure 36. How to remove bearing housing assembly*

With this solution the position of the friction clamp in relation to the yoke is only determined by the clearance of the four fastening bolts. The clearance between the bolts and the friction clamp translates into an uncertainty of repeatability. A positional guide on the yoke was therefore implemented, as seen in Figure 37.



*Figure 37. Positional guide on the yoke*

A light-weight and compact guide was milled from three millimetre aluminium and two mounting hole drilled. Two M3 holes were drilled and threaded into the yoke and the guide plate bolted with two socket head bolts. The guide plate creates an edge, which the friction plate is pushed against. It helps the user to bolt the friction clamp straight every time on the yoke. The position along the edge was deemed less important as the test-bearings housing is not constrained on the shaft in axial direction.

The friction clamp was fastened to the yoke and measured for perpendicularity to the yoke until satisfactory. As the loading force cell was calibrated to take the weight of the sub-assembly below it into account, adding the aluminium piece and the two bolts on to the yoke adds an offset to the loading measurement of about 1 N, which was neglected.

#### **4.4.5. Assembly of oil system**

When assembling the oil system it was discovered that the oil tank was positioned too low in relation to the lower shelf, making it hard to fit any pipes below it. This occurred due to the T-coupling under the tank needing a ½” adaptor, which had not been accounted for in the CAD-model. Two spacers were manufactured to elevate the tank, while the adaptor was shortened as much as possible in a lathe. The pipes were run and insulated.

#### **4.4.6. Installation of electrical cabinet**

The cabinet was mounted to two flat steel bars, which were then bolted to the wall, below an existing electrical cabinet, as seen in Figure 38. Cable ladders were placed for cabled running between the electrical cabinet and test-rig.



*Figure 38. Installation of electrical cabinet*

## **4.5. Software**

For the controlling of the test rig, a program was written in Matlab. The software environment was chosen as it lowered the threshold for development time, with toolboxes available for the National Instruments (NI) DAQ chosen as well as OPC.

### **4.5.1. Method**

Much focus was initially placed on making a robust and user-friendly program, with fully functioning error detection, error correction and results evaluation capabilities. As the thesis progressed the time plan was continuously reassessed, forcing a reduced scope. Furthermore, the controller for the servomotor received was not the ordered model, lacking support for OPC. Troubleshooting, as to why OPC was not working as expected, added some delays. This forced the scope of the software to further shrink, in order to meet the thesis deadline. Only basic error detection for the servo motor was implemented, instead letting the user ascertain the details and the resetting of the error in the servo motors own software, IndraWorks Engineering. The software was developed bottom-up, with low-level functions written first in order to meet stages. These stages were:

- Connecting to NI DAQ
- Sending and acquiring data with NI DAQ
- Connecting to servomotor
- Sending parameters, triggering commands and reading status to and from servomotor
- Clean-up when closing software
- Design anonymous functions for handling data acquisition
- Converting between voltage and real measurement unit
- Saving and reading data to files
- Checking if emergency stop has been tripped or reset
- GUI to define the test cycle
- GUI to set pressure; display current loading, temperature and pressure and to start a test
- GUI operations while running a test and after finishing a test

Each function was documented initially to define the inputs and outputs before writing the function. Several small functions were created in order to clean up the code-base.

### **4.5.2. Servo controller**

The received servomotor controller was fitted with an optical connection, instead of a RJ45 connection. It also lacked support for PLC, which was internally used in order to offer support for OPC. After discussions with the manufacturer for the servomotor this was solved by shipping a new controlling unit. While delivery was on the way, the communication was implemented via serial RS232. The correct controlling unit was then received and allows future features to be implementable.

### 4.5.3. Features

When starting the program, it automatically checks that the required licenses are present in Matlab and attempts to create a session with both the NI DAQ and servomotor. The servomotor is then checked for errors and if successful launches a GUI, as seen in Figure 39.

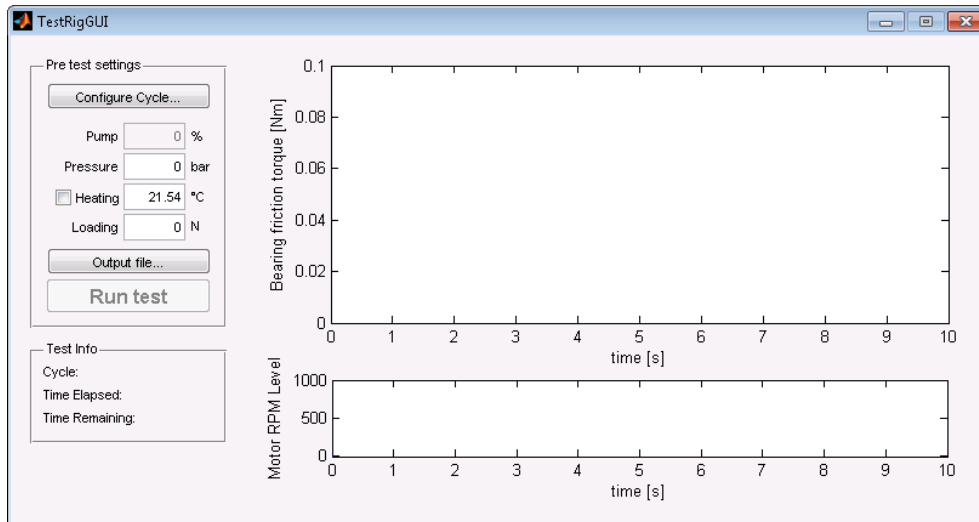


Figure 39. The main GUI of the program

At this point the user is not allowed to start the pump. By pressing *Configure Cycle...* the user must first configure the test cycle, as seen in Figure 40.

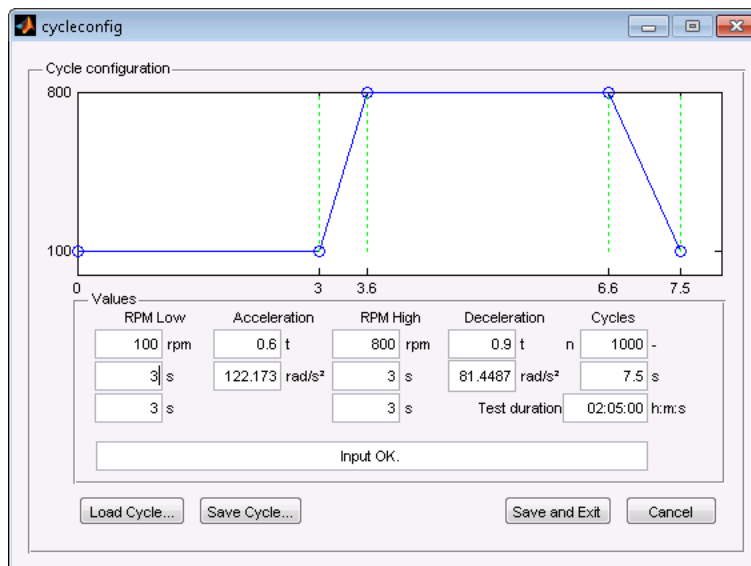


Figure 40. Configuring the test cycle

The user enters the parameters of each part of a four-step cycle, the low-rpm step, acceleration step, high-rpm step and deceleration step. Each input is checked for validity and against the capabilities of the servomotor. After configuring a cycle it may be saved for future use. When a cycle has been configured, the user is allowed to enable the pump, as seen in Figure 41.

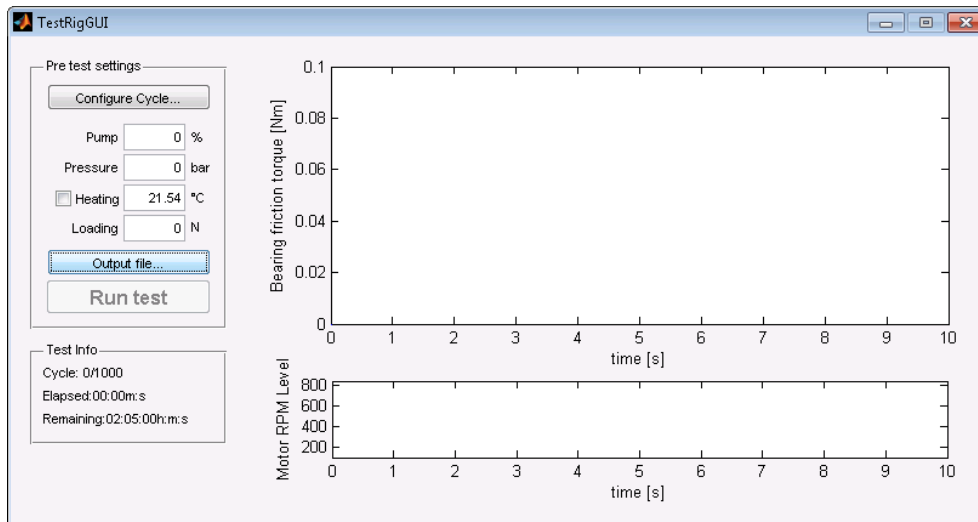


Figure 41. The main GUI with pump enabled

The user must then choose where to save the test data in order to be allowed to start a test. When initiating a test, the system captures five seconds of data on the friction loading test cell in order to calibrate the offset of any built-in forces. All other sensors feature pre-calibrated offsets.

Should a user choose to abort a test, the program will gracefully stop the test and reset to a state where a new output file needs to be selected before starting a test.

Should the emergency stop be triggered, the test-rig will immediately stop. The software responds with a fatal error and requires a restart. The emergency stop and servomotor need to be reset before starting the software. Should an error persist, the program will inform that it encountered an error, at which stage and how to rectify it.

## 5. INITIAL TESTING AND EVALUATION

In this chapter the initial testing of the rig and the evaluation of the function is discussed.

### 5.1. Electrical wiring

After installing the electrical cabinet, the programming was started. Initially the functions of the cabinet were validated. It was gathered that two of the sensors were not functioning as anticipated. The temperature and pressure sensor had mistakenly been installed as active sensors, as described in Figure 42, while they should have been installed as passive.

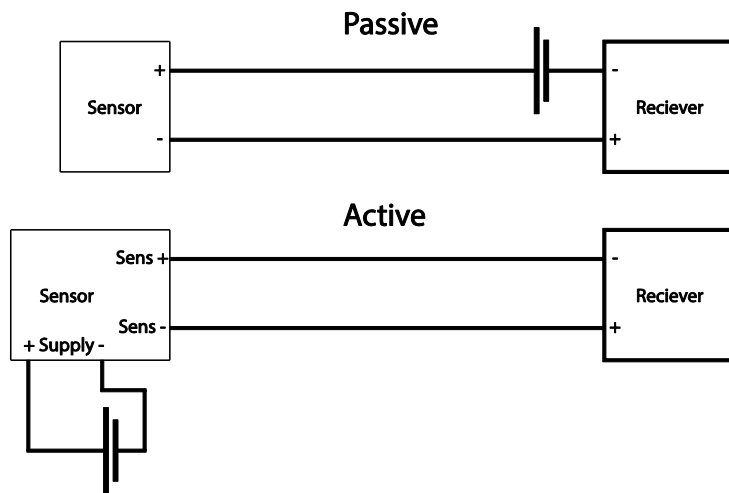


Figure 42. Passive and active equipment explained

The wiring was corrected and drawings for the electrical cabinet updated.

### 5.2. Noise and spikes in gathered data

When gathering data, the noise to signal ratio was assessed and while the general noise level was quite low, there was a problem with intermittent spikes of noise, as seen in Figure 43.

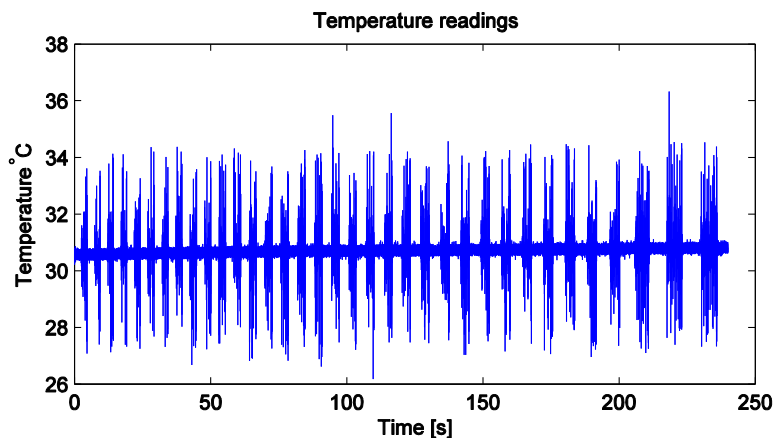


Figure 43. Noise spikes while running the pump

This was attempted to be fixed with a low-pass filter in Matlab, but this was not possible due to the relatively low sampling rate of 1 kHz. After troubleshooting the pumps frequency inverter, as seen in Figure 44, was identified as the cause.

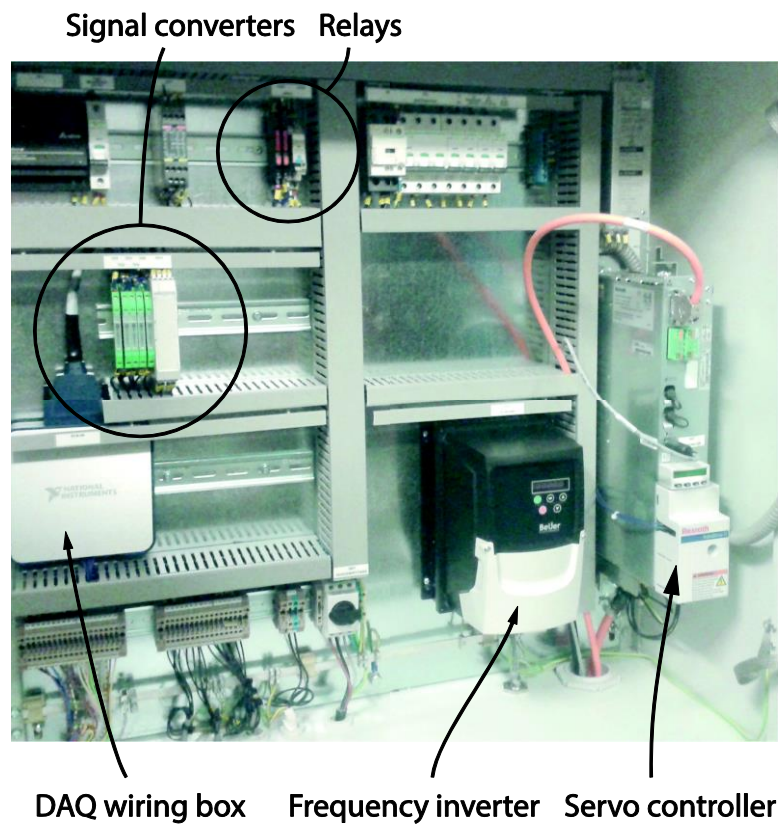


Figure 44. The major components in electrical cabinet

An oscilloscope and a wand capable of measuring electromagnetic fields were used to assess if there could be other sources of interference. The frequency inverter however was the lone source of any major EMR. Readings showed that the EMR was largest below and to the right of the frequency inverter. This was attributed to the cover of the inverter being plastic, while the switching transistors were placed on the right with power cabling exiting the bottom.

When controlling the pump, a voltage signal is sent from the DAQ wiring box to a signal converter, which in turn connects to the frequency inverter. The section between the signal converter and frequency inverter was fitted with several layers of shielding and a low-pass filter. While the cable to the pump itself was shielded, the wires between the cable gland and the frequency inverter were not, and these were shielded as well. While the EMR did indeed decrease, it did not translate into a less noisy data acquisition.

A shield for the frequency inverter was designed and implemented, as seen in Figure 45.



*Figure 45. Shield over frequency inverter installed*

This did indeed reduce the EMR to the levels of the room in general. The spikes in the data acquisition were however still present. Measurements on the signal cable showed low levels of interference, indicating that the noise was propagating via another cable. Measurements with the oscilloscope showed that the logical signal cable, travelling to the breaker and back, had significant amounts of interference. This cable was used to allow the user to logically turn the pump on and off. The cables were disconnected and the outputs bridged. This removed almost all intermittent noise in the data acquisition, as seen in Figure 46.

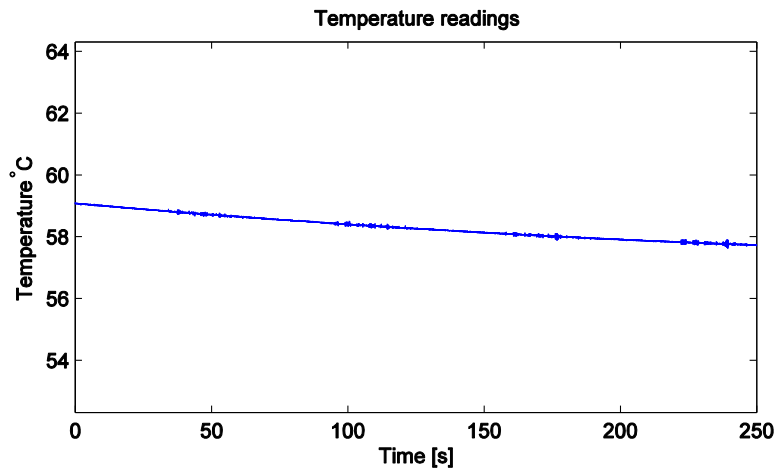


Figure 46. Signal without noise from frequency inverter

The remaining intermittent noise is believed to be caused by the controller for the servomotor, but as the amplitude is much lower, this has not been addressed. As the feature to have an enable-disable button for the pump can be worked around, by setting the pump to lowest value, the breaker was disabled.

### 5.3. Friction torque load cell misalignment

After assembling the loading mechanism, it was discovered that the friction torque load cell and friction sheet, as seen in Figure 24, did not align as anticipated, as seen in Figure 47.

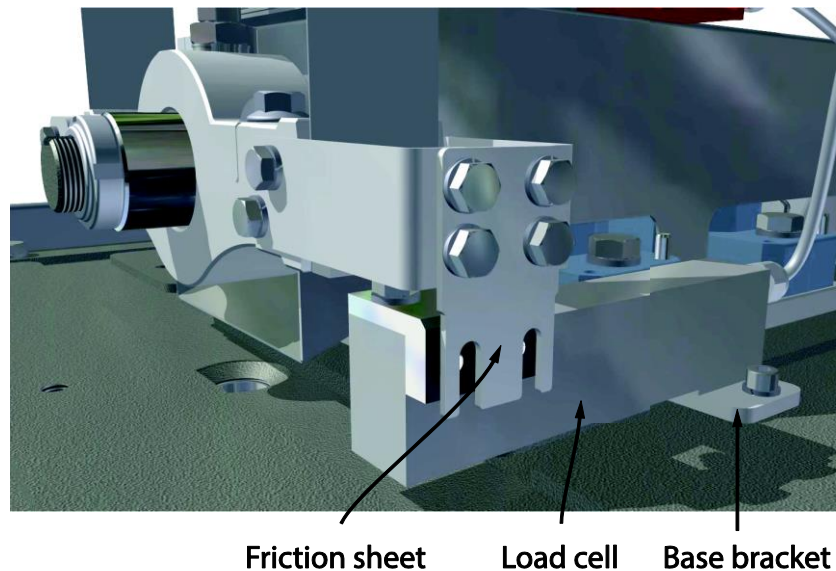
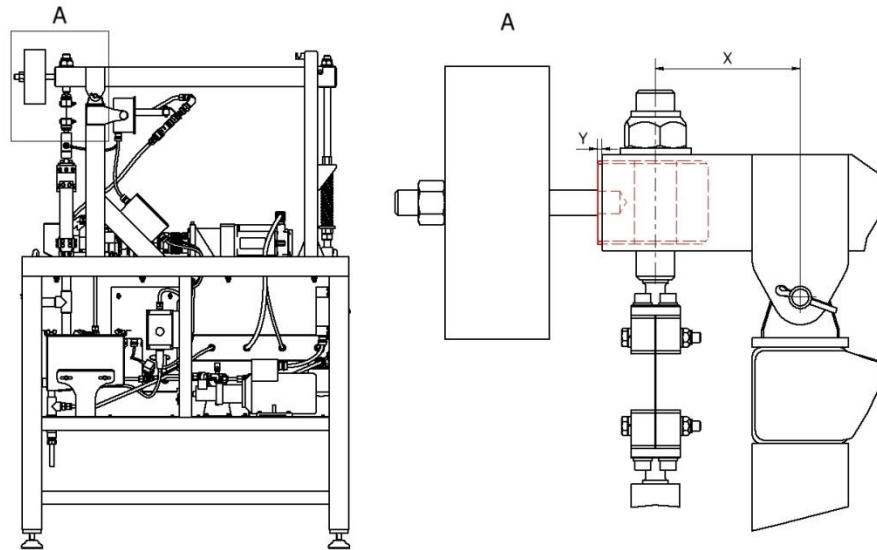


Figure 47. Misalignment of friction sheet

After taking measurements it was discovered that the test-bearing housing was about three mm closer to the support bearings than stated in the drawings. After troubleshooting, assembly error was ruled out and instead attributed to manufacturing error in the loading arm. The insertion piece, marked in red in Figure 48, was incorrectly welded flush to the end of the loading arm.



*Figure 48. Manufacturing error in the loading arm*

The hole was positioned three mm closer to the pivot than noted in the drawings. This was due to measuring the drilling position from the end of the profile, resulting in the specified distance  $X$ , as shown in Figure 48, being wrong. This error in turn misaligned the friction sheet in relation to the friction torque load cell.

It was noted from manufacturing that the error had been made, but that all dimensions should be correct. In order to solve this error a new bracket for the friction torque load cell, which took this misalignment into consideration, was made. The bracket was made to be adjustable by having elongated holes, which allows the friction torque load cell to slide axially with the shaft.

## **5.4. Oil splash**

During initial testing it was discovered that oil, when above ambient temperature, was leaking out through the clearance between the oil splash cover and shaft. The gap is seen in Figure 49.

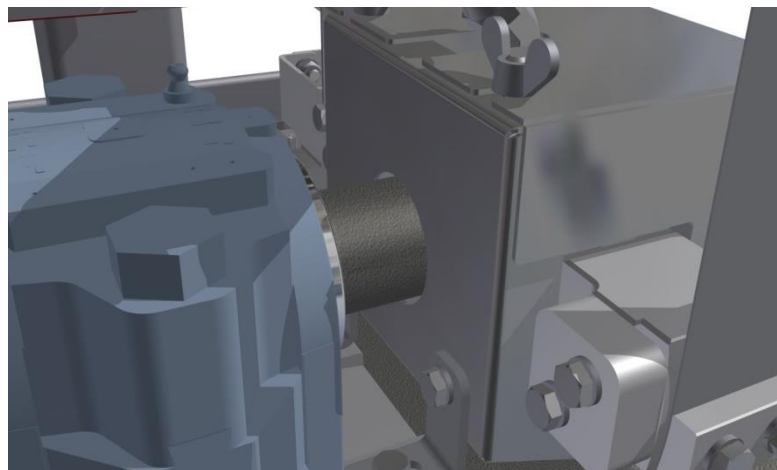


*Figure 49. The clearance between shaft and oil splash cover*

The emergency stop breaker at the door was disabled, in order to gain insight to what happening. With oil temperature set to 40 °C, the oil splash cover was removed in order to better investigate the test-bearings side leakage. The side leakage was escaping as four streams at the point where the bearing shells were mating, as seen in Figure 50.



*Figure 50. Oil spewing out of bearing*

The splash cover did not catch this and the oil spewed onto the labyrinth seal of the closer support bearing. Concern was raised that oil would enter the bearing housing, with unknown consequences to the grease lubrication. After an hour long static test, the support bearing was opened and small traces of oil was identified. It was assessed that longer tests would introduce significant amounts of oil into the support bearing housing.

Ideas on solving the leakage were discussed and evaluated, with a priority on simplicity and implementation time. A simple solution was to place an O-ring close to the clearance in order to break up the oil jets, as seen in Figure 51.

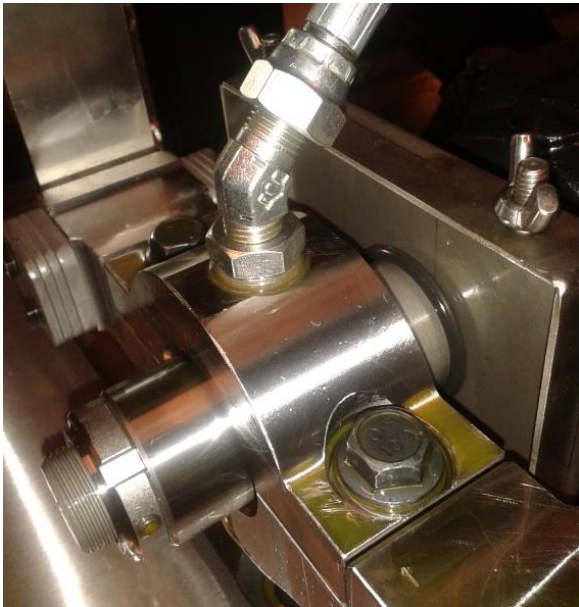


*Figure 51. O-ring installed close to the clearance of the oil splash cover*

The solution showed to work very well and almost no oil longer leaked through the clearance.

## **5.5. Assembly and disassembly of test-bearing housing**

Although the design of the test bearing housing was completed during the AMD-course, it was still unclear how the assembly and disassembly procedure would most efficiently be done. Many unknowns, such as how easily the upper part of the test-bearing housing (seen in Figure 22) could be removed, remained. Two principle solutions for disassembly were investigated.

The first method was focused on keeping the disassembly as simple as possible. The user begins by unlocking the friction measurement screws, unloading the system and then finally removing the oil splash cover, in order to access the test-bearing housing. The flexible hose is then uncoupled and the two bolts securing the upper part of the test-bearing housing are removed. The upper test-bearing housing is then removed. The upper bearing shell is then easily removed, but access to the lower bearing shell is limited. The sleeve is removed by removing the lock nut and sliding it off the shaft. The lower shell is then accessible to be removed, as seen in Figure 52. To reassemble the process is reiterated in reverse order.

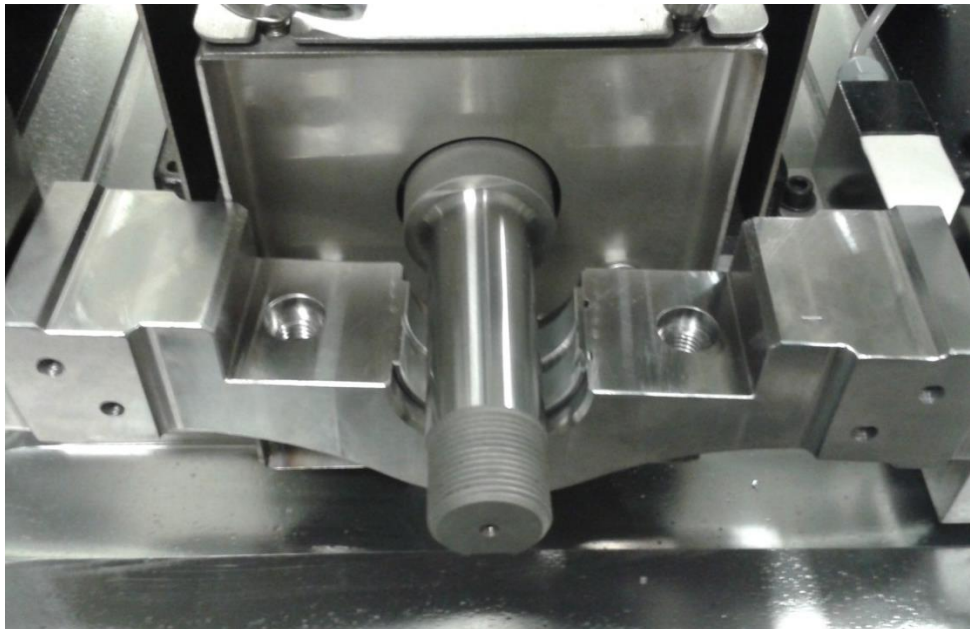


*Figure 52. Lowerbearing shell accessible after sleeve has been removed*

The second method shares the same first step of gaining access to the test-bearing housing. The lock nut, which secures the sleeve, is then removed. The flexible hose and the four bolts which hold the upper yoke are then removed. The whole subassembly, including the sleeve, is then slid off the shaft and placed on a table, as seen in Figure 53.



*Figure 53. The sub-assembly removed from rig when removing bearing shells*

The upper part of the test-bearing housing is then unclamped and removed, the sleeve removed, leaving the bearing shells to be easily removed. When reassembling, the process is done in reverse.

The bolts for the top of the test-bearing housing are tightened to 55 Nm, which, if using the first method, would put a considerable strain on the bearing shells as the shells are in contact with the shaft. This strain could possibly damage the surface roughness or cause plastic deformation of the evaluated shells. Solutions to hold the test-bearing housing, in order to reduce the stress while applying torque, were identified but not evaluated.

As the second method does not subject the bearing shells to any unwanted stress, it was concluded as the better option.

## 5.6. Oil splash safety breaker

Implementing the oil splash safety breaker was one of the last features to be implemented on the test-rig. During the design phase of the AMD-course, this feature was not accounted for. Two possible positions were assessed as acceptable, as showed in Figure 54.

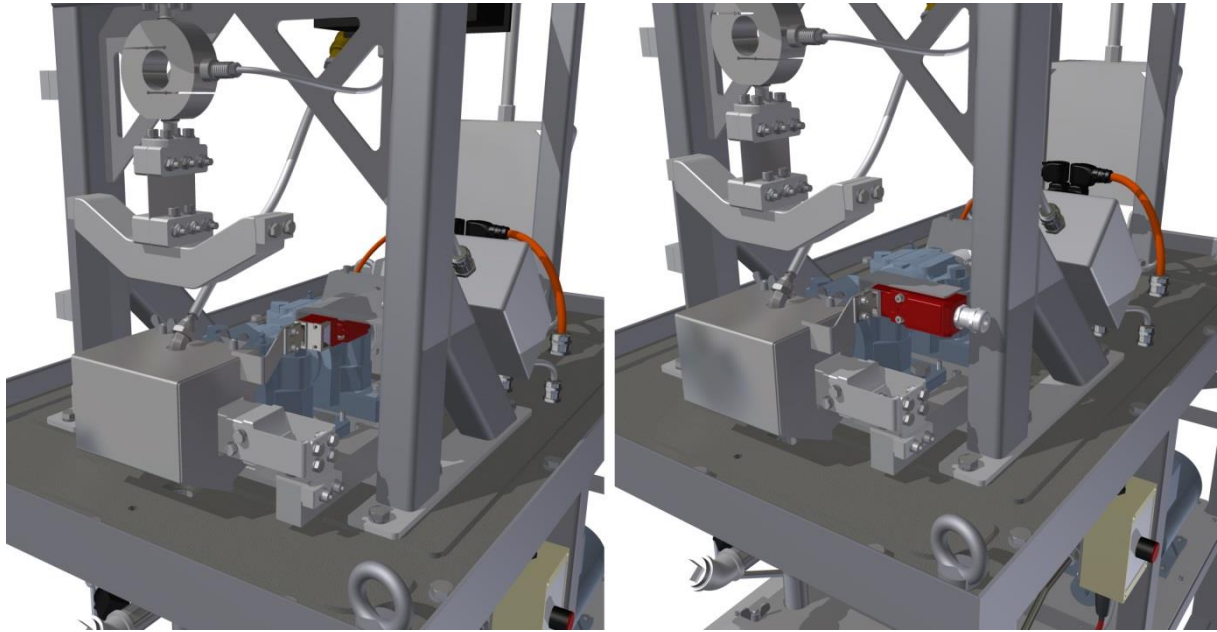


*Figure 54. Possible positions of oil splash breaker*

The main constraint was that the safety breaker was rated at a maximum operating temperature of 80 °C, while maximum oil temperature was specified at 150 °C in the requirements. Furthermore ease of cabling was assessed. The left version in Figure 54 positioned the safety breaker further away from the oil splash cover and was assessed as a bit more favourable. Cabling was also a bit simpler, as the cable went straight through the base-plate in one continuous bend. The cabling was, as best practice in safety equipment, physically separated from other signal cables, and as such the original thought out cabling paths had to be reassessed. Previously each load cell on the test-rig ran in separated cables, as seen in Figure 55, which was now not possible due to only having two cable glands through the base plate.

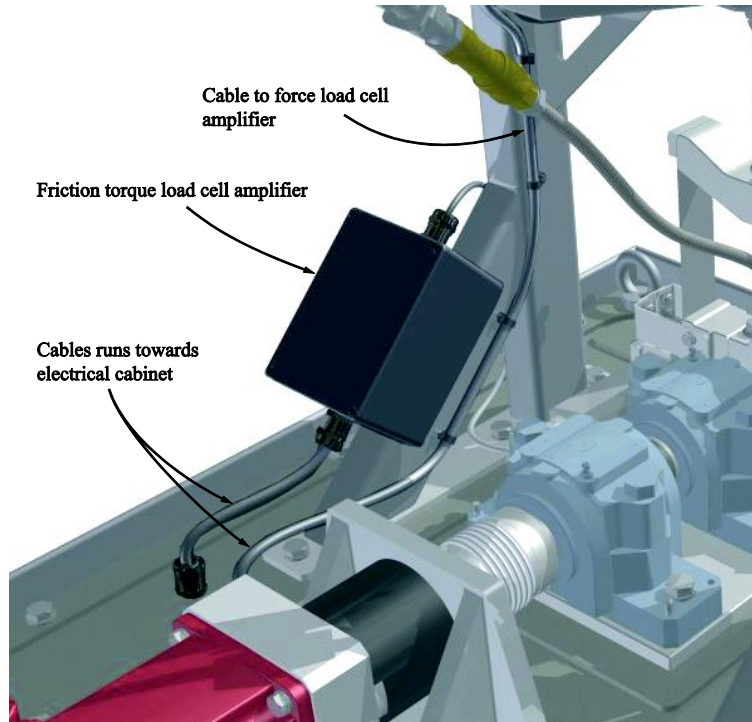


*Figure 55. Original cabling layout*

With the added cable for the safety breaker, the box containing the friction torque load cell amplifier was now additionally used as a junction box to combine the two cables into one slightly thicker cable, as seen in Figure 56, which was passed through the base plate.

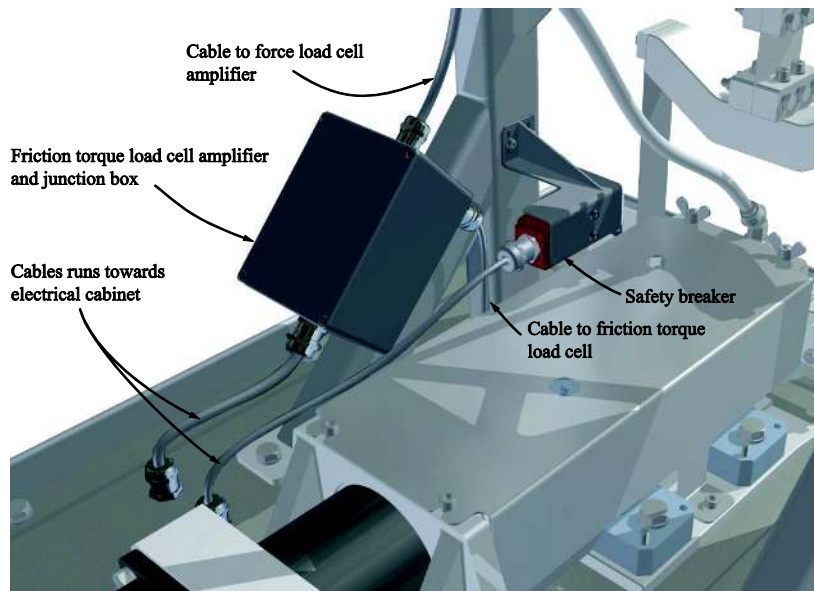


*Figure 56. Cabling after safety breaker was added*

## **5.7. Performance of oil system**

The performance of the oil sub system was evaluated as soon as all piping was completed. Five litres of 10w-30 engine oil was added to the oil tank and the pump started at a low velocity, in order to check for leakages. The pressure was brought up to eight bar(g) at ambient temperature, and after raising the temperature to 40 °C some leakage occurred at a few pipe connections. These connections were then further tightened.

The heating was then increased to test the temperature capability of the test-rig. At this point the oil sub system was not insulated and in order to speed up the test, the test-bearing housing was bypassed and the flexible hose was extended with a narrow tube which guided the oil directly into the hole in the base plate. After two hours the temperature converged at approximately 60 °C. In order to increase thermal efficiency and previously mentioned safety concerns, the oil system was insulated, as seen in Figure 57.

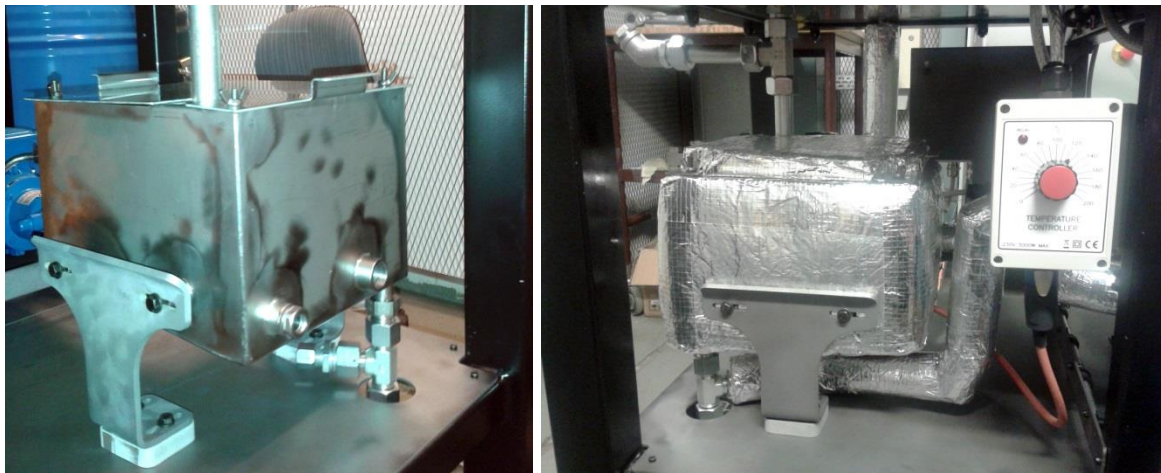


*Figure 57. Oil tank before and after insulation*

During the second test, the mean temperature increase was approximately 0.35 °C/min during the first two hours, but slowed down considerably after the oil had passed 65 °C. After four hours of continuous heating, the oil temperature levelled out at 72 °C.

With the oil at its maximum temperature, the maximum oil pressure was 4.5 bar(g) with a stationary shaft and an unloaded bearing housing. When the bearing housing was fully loaded the pressure dropped to 4.1 bar(g). This was caused due to the increased clearance between the shaft and upper bearing shell.

## **5.8. Evaluation of friction measurement concept**

After the servomotor and oil system were controllable, the friction torque measurement function was assessed. Simple software to acquire data from the NI DAQ was written, while the servomotor was controllable via the parameterisation-software supplied with the servomotor. The oil was circulated at 5 bar(g) and ambient temperature while the test-bearing was loaded with 1 kN. The shaft was accelerated from standstill to 1,000 rpm in 0.5 s, kept at constant velocity and then ramped down to standstill with the same deceleration. The measurement from the friction torque load cell was simultaneously plotted. At this point

however, routines for saving data had not been written and only real time plots were available. During the accelerating and decelerating phases, a change in measurement was identified, which proved that the Eindhoven concept and our implementation worked.

## 6. TESTING

*In this chapter we discuss how testing with the test-rig was planned.*

The tests were planned in cooperation with Scania. An important criterion was the repeatability of the test-rig. With the remaining time frame, three types of tests were chosen; a Stribeck curve test, a wear test and a wear progression test. The data of the test bearing and journal used are presented in Table 2.

*Table 2. Data for sleeve and bearing shells*

Radius, R (mm)	20
Width, W (mm)	22
Average radial clearance, C ( $\mu\text{m}$ )	25
Surface roughness, $Ra_{\text{bearing}}$ ( $\mu\text{m}$ )	0.3
Surface roughness, $Ra_{\text{sleeve}}$ ( $\mu\text{m}$ )	0.45

The captured data was filtered in order to smooth out remaining noise.

### 6.1. Stribeck curve test

The Stribeck curve test focused on assessing the friction torque measurement capabilities of the test-rig and to identify the different lubrication regimes. All the tests were run in a factorial design with two variables with two and four levels, and three replications, as seen in Table 3. The speed was increased linearly between start and end speed.

*Table 3. Input parameters for Stribeck curve tests.*

Starting speed (rpm)	0
Ending speed (rpm)	1,000
Duration (s)	60
Load (N)	500, 1,000, 3,000, 5,000
Oil temperature ( $^{\circ}\text{C}$ )	30, 60
Oil pressure (bar(g))	1.3
Repetitions	3

The oil temperature was set in order to assess the effect of the changed viscosity. The viscosity data is presented in Table 4.

*Table 4. Viscosity data for SAE 10W30 oil used*

Dynamic viscosity, 40 $^{\circ}\text{C}$ (Pa·s)	$57.9 \cdot 10^{-3}$
Dynamic viscosity, 100 $^{\circ}\text{C}$ (Pa·s)	$11.3 \cdot 10^{-3}$

Testing was done for each temperature in series, while load was randomised for each replication with RANDOM.ORG's list randomiser (RANDOM.ORG, 2014), as presented in Appendix B. The oil pressure selected for the test corresponded to approximately half of the oil pressure in a truck engine running at 1,000 rpm (Spiegelberg, 2014). During testing of the low temperature level the lower bearing shell was replaced every fourth test, while one bearing shell was used throughout all the high temperature level tests. While randomising

temperature would have optimal, this was motivated by the fact that cool down and reheating would take too long time between tests at the elevated temperature. The upper bearing shell was not exchanged as it is not in contact with the sleeve during testing, and as such does not wear. The input parameters were used to calculate the dimensionless film parameter, in order to predict at what speed a full film lubrication regime would likely be fully developed. The dimensionless film parameters accuracy was then assessed with the data collected from the tests. Stribeck curves were calculated using the captured data for frictional torque, load and viscosity. Temperature readings were used to calculate the viscosity during the cycle. The Stribeck curves were passed through a low-pass filter and residuals were calculated.

## 6.2. Wear test

The wear tests purpose was to assert if the test-rig would produce wear on the test-bearings and how the wear was affected by different input parameters during starting and stopping conditions. The parameters for the wear test, seen in Table 5, features a  $2^2$  factorial design with replication on two random tests, in order to assess repeatability.

*Table 5. Input parameters for wear test*

Number of cycles (-)	10,000
Low speed (rpm)	0
High speed (rpm)	700
Load (N)	1,000, 5,000
Oil temperature (°C)	60
Oil pressure (bar(g))	0.9

The design is presented in Table 6.

*Table 6. Test design for wear test*

Test	Cycle	Load (N)	Test duration (h)	Test order
1	1	1,000	14,7	4
2	1	5,000	14,7	3
3	2	1,000	11,9	2
4	2	5,000	11,9	1
5	1	1,000	14,7	6
6	2	5,000	11,9	5

The pressure represents half the pressure of a truck engine at 700 rpm (Spiegelberg, 2014). A higher temperature was chosen in order to induce more wear, as the decreased viscosity results in a thinner oil film. The cycles used are presented in Table 7 and further described in Figure 58.

Table 7. Cycles described

Cycle	Time (s)					Cycles per hour (-)	Total test time (h)
	Low speed (t1)	Acceleration (t2)	High speed (t3)	Deceleration (t4)	Cycle time		
1	0.88	1.76	0.88	1.76	5.28	682	14.7
2	0.39	1.76	0.39	1.76	4.30	837	11.9

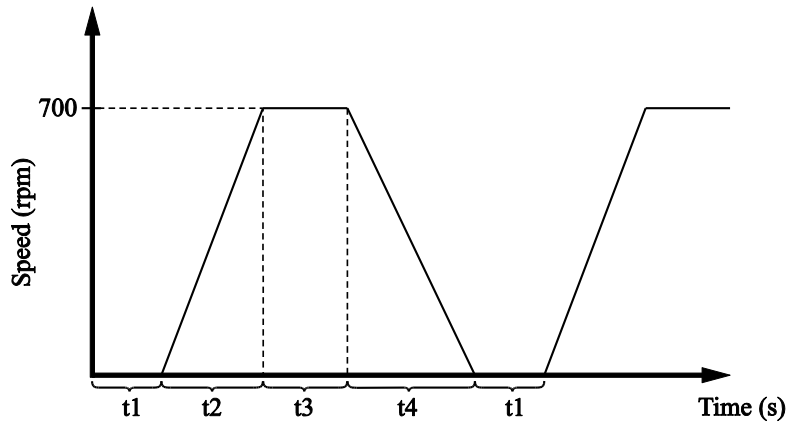


Figure 58. A test cycles components

For each test new measured bearing shells are used. These are then measured after a test in order to measure the wear volume and wear depth.

### 6.3. Wear progress test

The wear progress test aimed to give insight to the progress of wear in a wear test. Tests are conducted by running a number of cycles, and then measuring wear and reiterating the test in order to assess wear over time, as described in Figure 59.

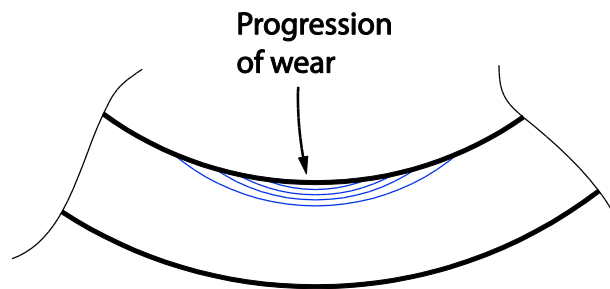


Figure 59. Example of wear progression on a bearing shell

Sub-tests, to those used in the wear test, are utilised for the wear progress test. Between each sub-test, the test-bearing is extracted and measured for wear. Each sub-test is progressively longer, as presented in Table 8.

*Table 8. Iteration times for each sub-test*

Iteration	Test duration (h)
1	1
2	3
3	5
4	10
5	50

Which cycle and parameters to use for the test was evaluated from the test results gained during the previous wear tests, as to choose the parameters which gained the most wear per hour.

## 7. RESULTS

*In this chapter we present the results of the testing.*

### 7.1. Stribeck curve test

The Stribeck curves were passed through a low-pass filter and residuals were calculated. These all showed non-uniformity and time-dependant oscillation, as seen in Figure 60, indicating that the error is likely speed dependant.

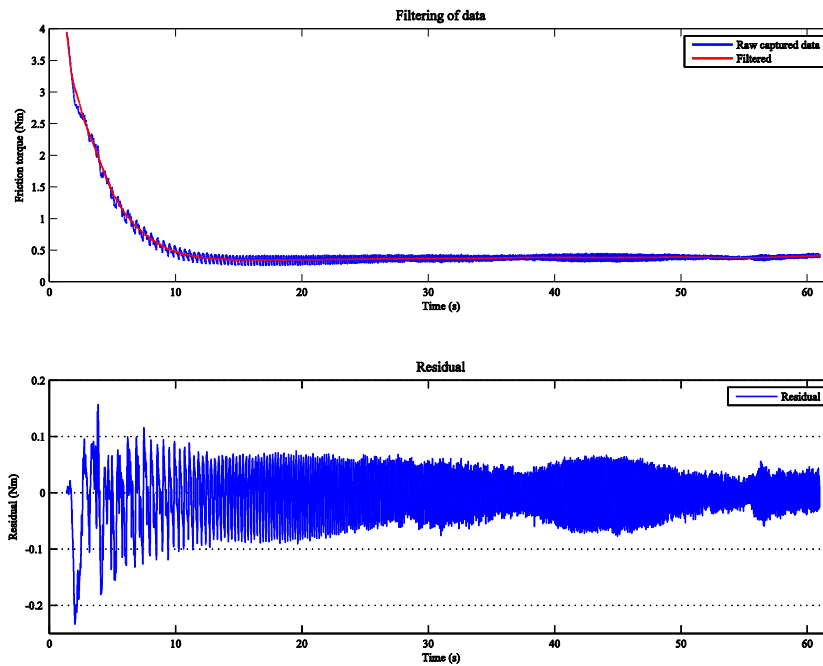


*Figure 60. Filtering of data and the residual*

There was no discernable difference in residual amplitude at different loads, suggesting that the spring-loading does not contribute to the noise frequency or amplitude. A general thickness of the residual is seen, suggesting that there are no major issues with natural frequencies.

The measurements show, as shown in Figure 61 and Figure 62, clear resemblance to traditional Stribeck curves.

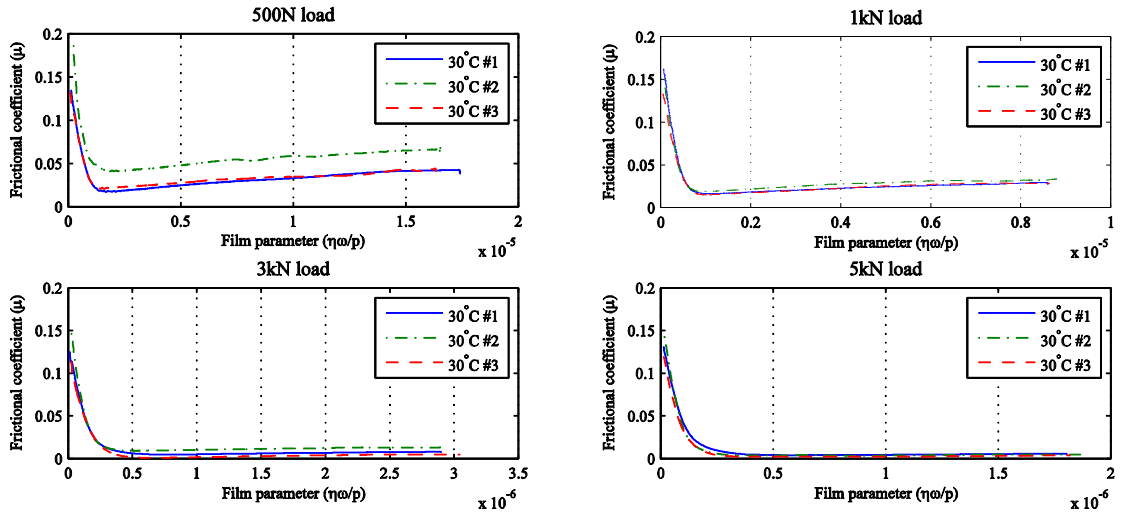


Figure 61. Stribeck curves for tests run at 30 °C with varying loads

An initial friction of 0.10-0.20 seems to correspond fairly well to typical friction values, around 0.15-0.30, for clean surfaces in contact for similar material combinations (Institutionen för Maskinkonstruktion, 2008).

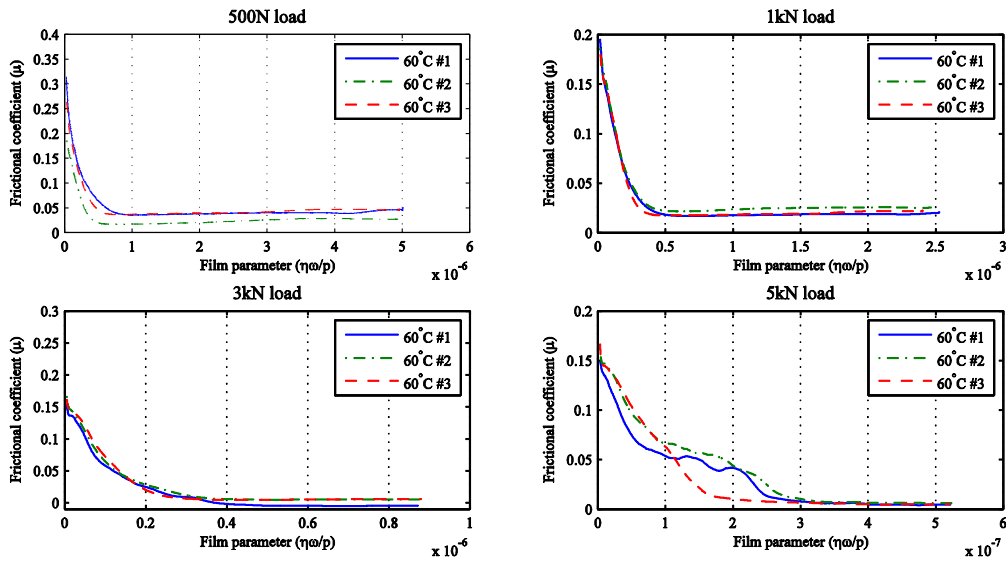


Figure 62. Stribeck curves for tests run at 60 °C with varying loads

Frictional values at elevated temperature range between 0.15 and 0.3.

There are some variations between tests, specifically test number two run at 30 °C and 500 N as well as all tests run at 60 °C with 5 kN loading are suspicious.

When plotting the most representative replication out of each test for 30 °C with speed on the x-axis, as seen in Figure 63, it can clearly be seen that there is a transition point where the samples diverge.

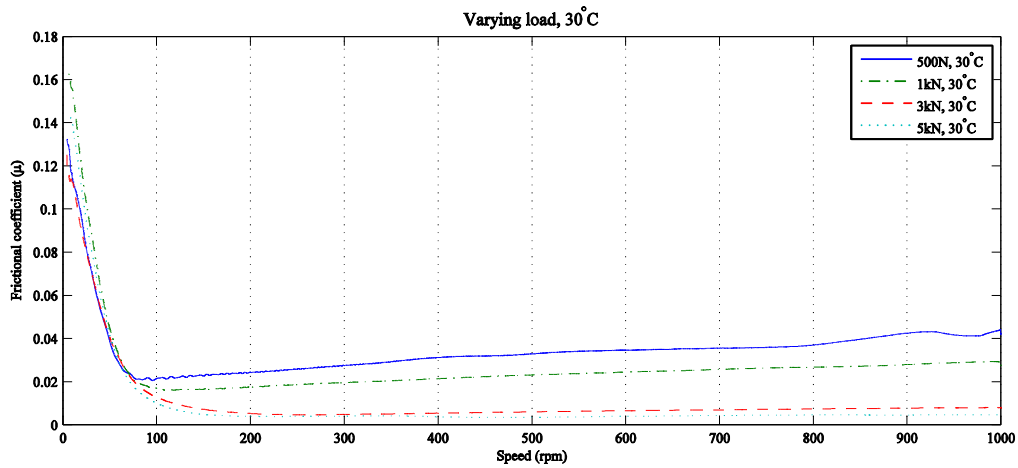


Figure 63. Different levels of loading at 30 °C

This seems to be the point where the film starts to carry a significant part of the load and the progression towards this point is not significantly influenced by loading. For 60 °C, as showed in Figure 64, this transition is not as clear.

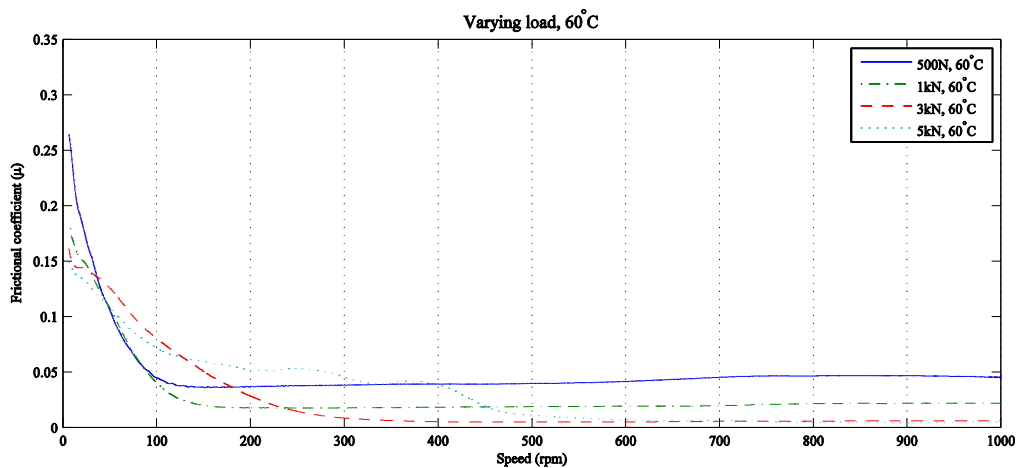


Figure 64. Different levels of loading at 60 °C

When plotting with the film-parameter, as seen in Figure 65 and Figure 66, the influence of the load is more clearly observed.

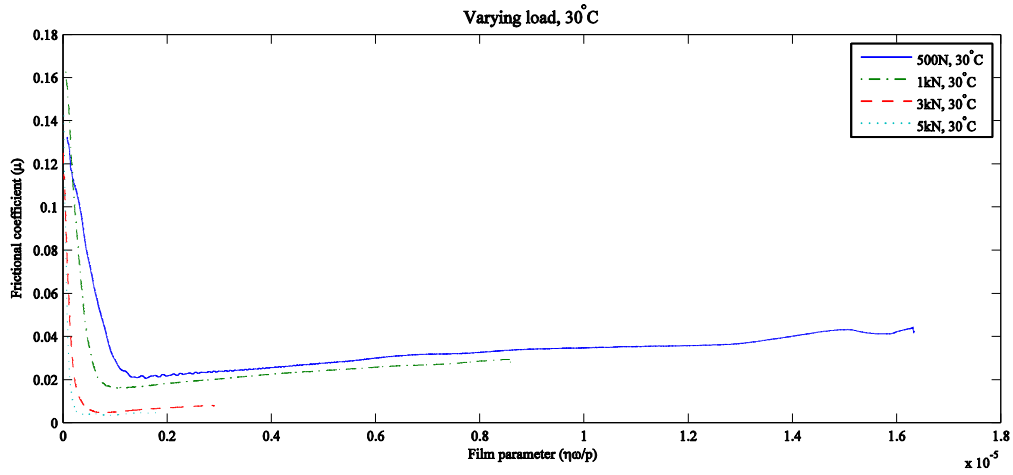


Figure 65. Frictional coefficient plotted against film parameter at 30 °C

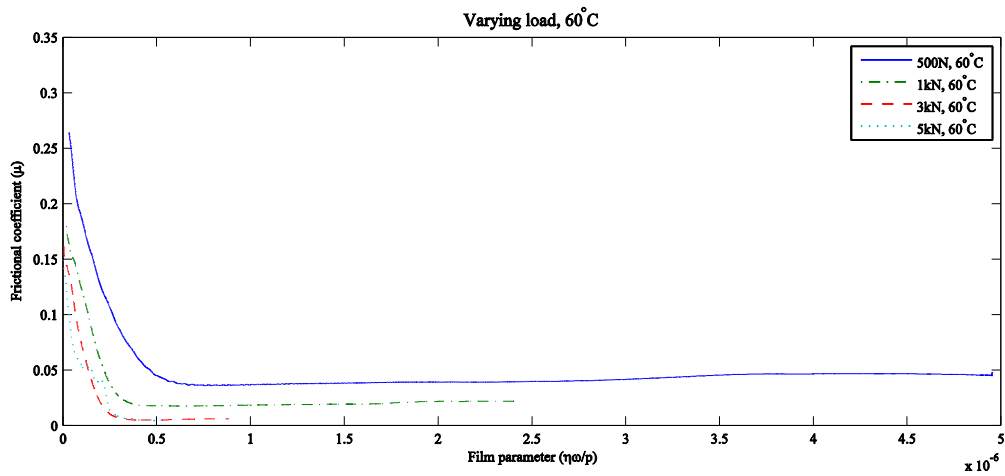


Figure 66. Frictional coefficient plotted against film parameter at 60 °C

It can clearly be seen that frictional values increase for all cases when temperature is increased, as the lowered viscosity forms a thinner film. Wear was visible on the bearing shells, but no measurements were taken.

Evaluation of the film parameter, as shown in Figure 67 and Table 9, made predictions for when the full film lubrication regime would be fully developed, ranging from 20 rpm to 741 rpm for different temperatures and load cases. The range between 3 and 4  $\lambda$  show where entering the hydrodynamic lubrication regime is predicted.

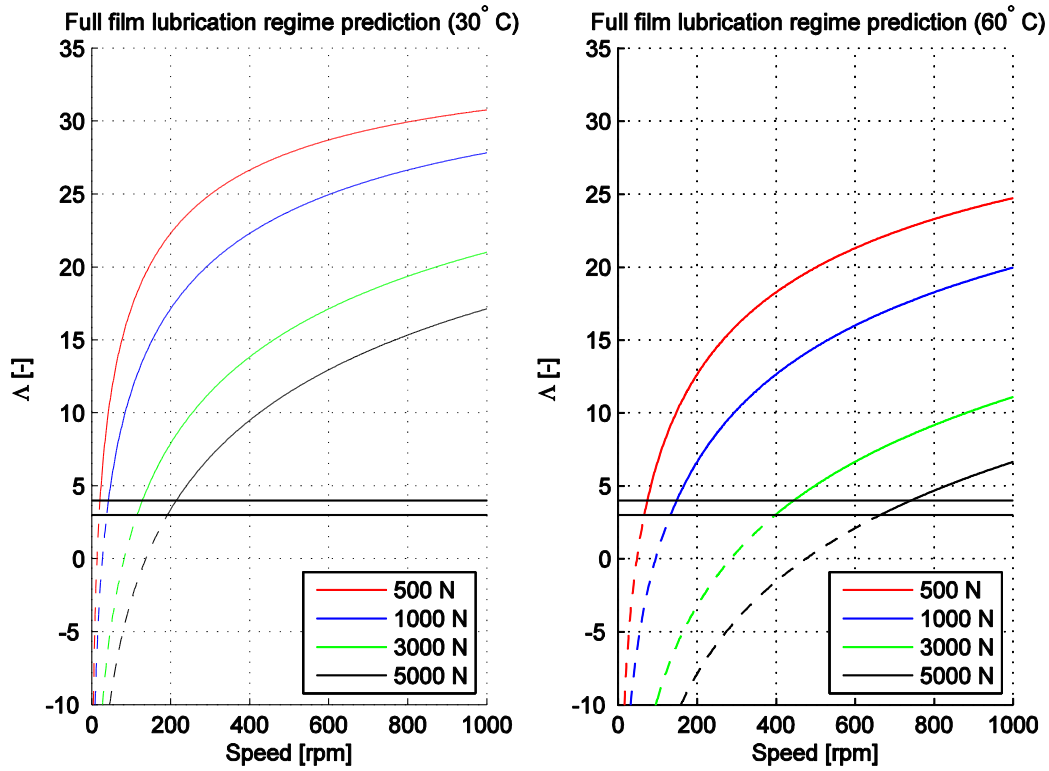


Figure 67. Plotting of full film parameter,  $\Delta$

Table 9. Predictions of when the full film regime would be fully developed

Load (n)	Prediction at 30 °C (rpm)	Prediction at 60 °C (rpm)
500	20-21	67-74
1000	39-42	133-148
3000	116-128	398-445
5000	193-214	664-741

Inserting the mean value of the predictions onto Figure 63 and Figure 64 yields Figure 68. The predictions are shown as crosses on the lines of their corresponding load case.

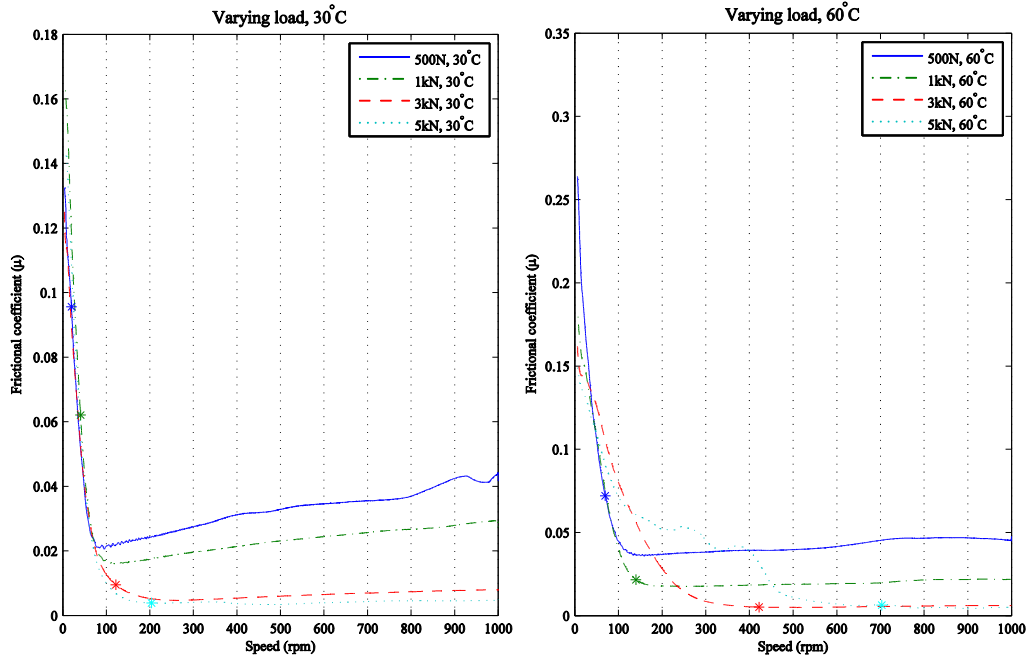


Figure 68. Predictions plotted onto Stribeck curves

It is clear that the predictions are fairly coarse, with better predictions as load increases.

## 7.2. Wear test and subsequent damage of test-rig

After the first wear test was completed it was discovered that the machine had become damaged. During the 12h cycle the guiding bearing lost its grip on the shaft, allowing it to travel axially, causing damage to the non-guiding bearing. The chamfer on the shaft, located between the support-bearing housings travelled towards the labyrinth seal, ultimately gripping onto it and forcing it to abrasively grind against the bearing housing. This continued until the bellows-coupling was compressed enough to cause equilibrium in axial direction. The labyrinth seal was forced approximately one centimetre into the support bearing. The result, as seen in Figure 69, was an axial displacement of approximately two centimetres.

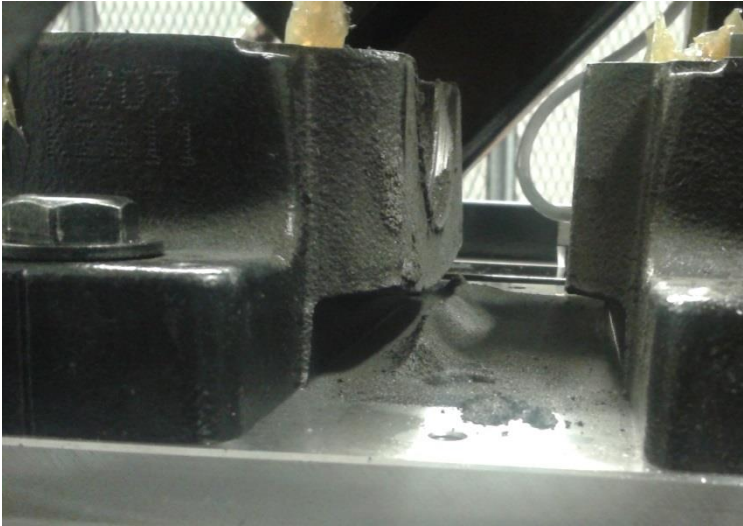


Figure 69. Overview of damaged support bearing housing

Furthermore, both support bearings are heavily contaminated with metallic particles, as seen in Figure 70, while one of the bearing housings is destroyed, as seen in Figure 71.



*Figure 70. View of contaminated bearing and damaged bearing housing*



*Figure 71. Powder created by grinding of the bearing housing*

The shafts radius at the chamfer, as seen in Figure 72, was destroyed as well as surfaces at the bearing locations.



*Figure 72. View of destroyed inner radius at chamfer*

The oil system was also heavily contaminated by the metallic dust created, causing approximately 80  $\mu\text{m}$  of wear to the test-bearings surface during 10,000 cycles, a substantial amount.

## 8. DISCUSSION AND CONCLUSION

---

*In this chapter we discuss the results of the thesis.*

### **8.1. Discussion**

The project aimed at building a functioning test-rig which could be used for further studying journal bearings during transient states. This was not achieved, due to damages accrued during testing. Before the test-rig can be said to be in an operational state, a fault analysis needs to be conducted and suggested changes from it implemented.

The Eindhoven-concept (Peels & Meesters, 1996) has been proven to work well, with testing prior to damaging the test-rig showing promising results. Frictional values and trends correspond well to known frictional values (Institutionen för Maskinkonstruktion, 2008, p. 88) and hydrodynamic film theory (Beek, 2009, p. 275). All tests showed that the test-rig is able to produce wear. The test-rig has shown good repeatability in the tests ran, but with a few outliers. Furthermore, one result showed a negative friction coefficient. This is likely due to a small backlash in the friction torque measurement system, with the offset recorded at an unfavourable case. It is also uncertain how the strain energy of the frictional torque is distributed between the flexible connection and friction torque load cell.

The heating and pump capabilities of test-rigs do not match the requirements. The oil temperature could only be brought up to 72 °C, with a pressure of 4.2 bar(g), while specifications state 150 °C at 5 bar(g). Increasing heating will furthermore decrease the maximum pressure attainable. The pump has an influence of the temperature, influencing the temperature approximately two to three centigrade. The pump and heating affect each other, where an increased pressure increases temperature, due to increased friction in the pump, which causes the viscosity of the oil to drop, causing the pressure to drop. The latency in the heating of the oil system further worsens the accuracy.

Signal noise, while not quantified, in the acquired data is almost negligible, thanks to filtering and the reduction of noisy sources. The acquired data is further refined by weighted local regression before evaluation. Delivery delays of the electrical sub-system forced much of the finer details of the software, such as robust automated handling of acquired data, intelligent error handling and automatic controlling of the oil pump, to be removed from the software planning.

In summary, the test-rig has shown promising results, but needs to be repaired before any further results can be attained. We have shown that the test-rig is able to produce wear on bearing shells and produce results which lie close to theoretical results. The test-rig can be used to further study the influence parameters have on transient states in a journal bearing.

## **8.2. Conclusions**

- The test-rig has been realised and evaluation shows good correspondence to frictional values at starting of similar material combinations.
- The test-rigs concept has been proven to work.
- The bearing shells that were used showed wear.
- Repeatability for the tests ran shows good consistency.
- The test-rig needs to be repaired before additional tests can be performed.

## 9. FUTURE WORK

---

*In this chapter we discuss the future of the project.*

- The cause of the failure of the test-rig should be analysed.
- The rig should be repaired.
- The shaft should be redesigned to include shoulders, in order to simplify assembly.
- The heating should be analysed and modelled in order to assess possible changes to the heating.
- The influence on the shaft and support bearings from additional heating should be investigated.
- The influences on the oil pressure, given implementation of a heating system which meets the requirements, should be investigated.
- A control system should be implemented for temperature and pressure control.
- Natural frequencies of the test-rig should be investigated in order to better understand the characteristics of the test-rig.
- A theoretical model of the test-rig should be created with AVL Excite.
- The repeatability should be further investigated.



## 10. REFERENCES

---

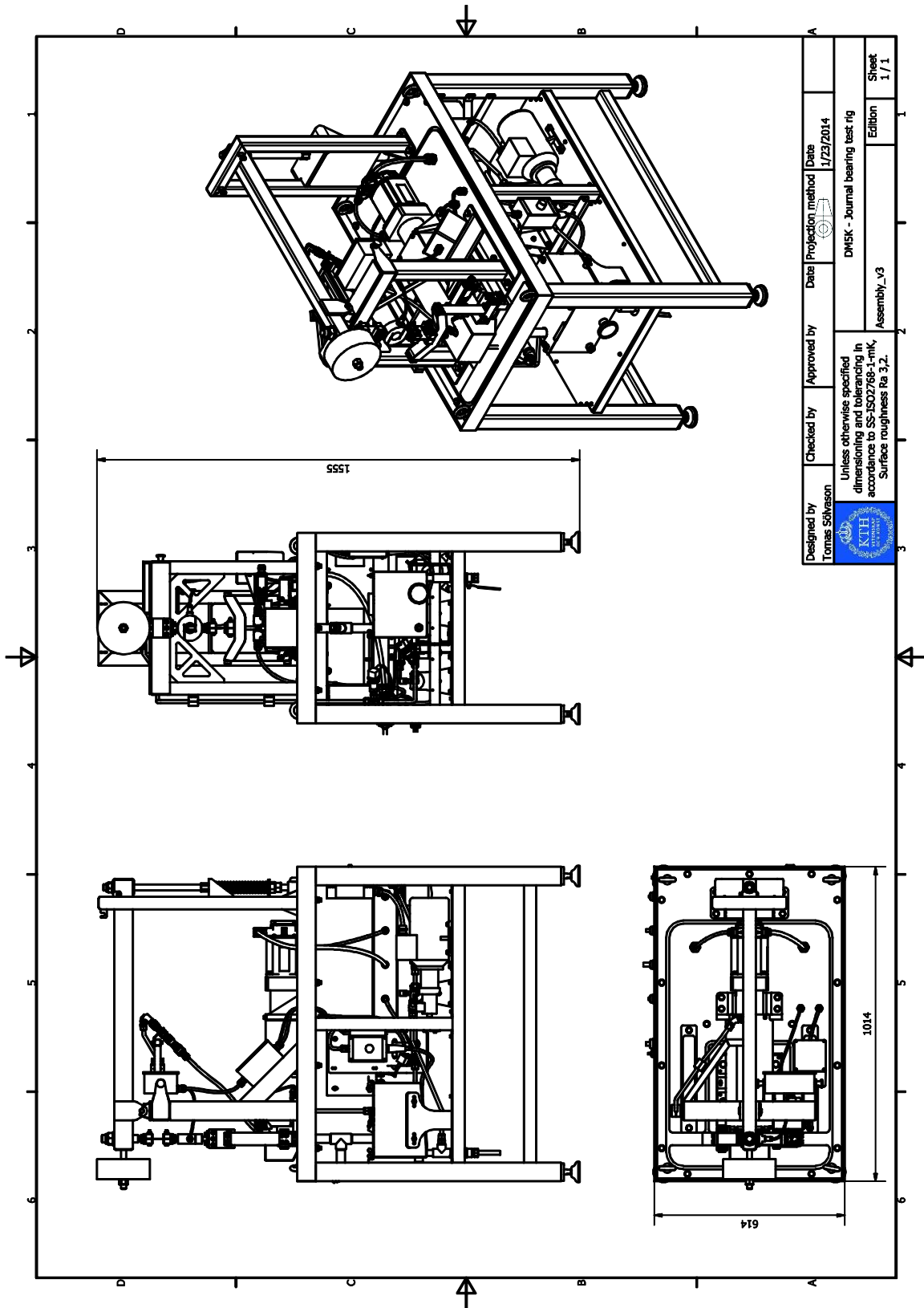
*In this chapter the references made in this work are listed.*

- ABB AB Jokab Safety. (2011, December 7). *Safety in control systems according to EN ISO 13849-1*. Retrieved May 29, 2014, from <http://www.abb.com/product/ap/seitp329/89cd7cad9f5586dec12579970036a679.aspx>
- Babbitt, I. (1839, July 17). *Patent No. 10954*. United States of America.
- Beek, A. v. (2009). *Advanced engineering design*. Delft: TU Delft.
- Dataforth. (2002, Februari 17). *Protecting Singal Lines Against Electromagnetic Interference*. Retrieved May 12, 2014, from <http://www.dataforth.com/catalog/pdf/an508.pdf>
- Eriksson, T., Folkesson, A., & Hagman, L.-A. (2001). *Maskinelement, Tribologi mekanismer*. Stockholm: Institutionen för maskinelement, Kungliga Tekniska högskolan.
- (2011). *Gas Turbine Engineering Handbook, Fourth Edition*. In M. P. Boyce, *Bearings and Seals* (p. 572). Oxford: Butterworth-Heinemann.
- Gudin, D., Mian, O., & Sanders, S. (2013). Experimental measurement and modelling of plain bearing wear in start-stop applications. *Proceedings of the Institution of Mechanical Engineers, Part J: Journal of Engineering Tribology 2013 227* (pp. 433-446). Sage.
- Harnoy, A. (2003). *Bearing Design in Machinery - Engineering Tribology and Lubrication*. New York: Marcel Dekker.
- Institutionen för Maskinkonstruktion. (2008). *Maskinelement handbok*. Stockholm: Institutionen för Maskinkonstruktion, Kungliga Tekniska Högskolan.
- Maylor, H. (2010). *Project Management Fourth Edition*. Essex: Pearson Education Limited.
- Mokhiamer, U., Crosby, W., & El-Gamal, H. (1998). A study of a journal bearing lubricated by fluids with couple stress considering the elasticity of the liner. *Wear, 224*, 194-201.
- National High Magnetic Field Laborator. (2014, June 4). *National High Magnetic Field Laboratory*. Retrieved June 4, 2014, from <http://www.magnet.fsu.edu/education/tutorials/tools/faradaycage.html>
- National Instruments. (2014, Feb 14). *Isolation Technologies for Reliable Industrial Measurements*. Retrieved Feb 19, 2014, from <http://www.ni.com/white-paper/3546/en/pdf>
- Nave, C. (1997, September 6). *HyperPhysics*. Retrieved May 31, 2014, from <http://hyperphysics.phy-astr.gsu.edu/hbase/magnetic/wirfor.html>
- Peels, J., & Meesters, C. (1996). Ontwerp en constructieve aspecten van een 2kN-glijlageropstelling. *De constructeur, 34(3)*, 40-43.
- RANDOM.ORG. (2014, June 2). *List Randomizer*. Retrieved from RANDOM.ORG: <http://www.random.org/lists/>

- Simmons, G. (2010). *20 years of hydro-dynamic journal bearing research: 1990 to present*. Luleå: Division of Machine Elements, Luleå University of Technology.
- Spiegelberg, C. (2014, May 30). Discussion on truck engines and bearing liners. (M. Galde, Interviewer)
- Tomanik, E., & Ferrarese, A. (2006). Low friction ring pack for gasoline engines. *ASME 2006 Internal Combustion Engine Division Fall Technical Conference*, 449-455.

# Appendix A. SIZE DRAWINGS

In this appendix we present size drawings of the test rig.





# Appendix B. TESTING PLAN FOR STRIBECK CURVE TEST

---

Test	Oil temp [°C]	Oil pressure [bar(g)]	Bearing load [N]	Shell number
1	30	1.3	500	1
2	30	1.3	3000	1
3	30	1.3	5000	1
4	30	1.3	1000	1
5	30	1.3	5000	2
6	30	1.3	500	2
7	30	1.3	1000	2
8	30	1.3	3000	2
9	30	1.3	3000	3
10	30	1.3	1000	3
11	30	1.3	500	3
12	30	1.3	5000	3
13	60	1.3	5000	4
14	60	1.3	500	4
15	60	1.3	3000	4
16	60	1.3	1000	4
17	60	1.3	3000	4
18	60	1.3	1000	4
19	60	1.3	500	4
20	60	1.3	5000	4
21	60	1.3	500	4
22	60	1.3	3000	4
23	60	1.3	1000	4
24	60	1.3	5000	4